Tectonophysics xxx (2016) xxx–xxx

Contents lists available at ScienceDirect

Tectonophysics

journal homepage: www.elsevier.com/locate/tecto

Impact of stylolites on the mechanical strength of limestone

Patrick Baud [a,*], Alexandra Rolland [a], Michael Heap [a], Tao Xu [b], Marion Nicolé [a], Thomas Ferrand [c], Thierry Reuschlé [a], Renaud Toussaint [a], Nathalie Conil [d]

[a] Institut de Physique du Globe de Strasbourg (UMR 7516 CNRS, Université de Strasbourg/EOST), 5 rue René Descartes, F-67084 Strasbourg Cedex, France
[b] College of Resources and Civil Engineering, Northeastern University, Shenyang, China
[c] Département de Géologie, Ecole Normale Supérieure, Paris, France
[d] Andra, Bure, France

ARTICLE INFO

Article history:
Received 4 November 2015
Received in revised form 11 January 2016
Accepted 8 March 2016
Available online xxxx

Keywords:
Uniaxial compression
Carbonates
Stochastic modelling
Microporosity

ABSTRACT

We performed a series of uniaxial compression tests on samples of microporous carbonates from the Paris Basin (Bure, France). Sedimentary stylolites are pervasive in these formations. We show that the porosity in the vicinity of the stylolites is always higher than that of the host rock. As a result, our new mechanical data reveal that samples with a stylolite are always measurably weaker with respect to the adjacent stylolite-free material. However, when present, the orientation of the stylolite (with respect to the direction of loading) does not result in any mechanical anisotropy. Numerical simulations using a 2D finite element code suggest that the weakening induced by the presence of a stylolite is mostly due to the higher porosity and the higher level of heterogeneity in and around the stylolite, while the absence of mechanical anisotropy is due to the roughness of the stylolite. While the presence of stylolites weakens carbonate rocks, stylolites only act as planes of weakness when their thickness exceeds a certain threshold (about 5 mm).

1. Introduction

Stylolites are the product of intergranular pressure-solution and are common in sedimentary formations. They have been described in carbonates (Stockdale, 1943; Park and Schot, 1968; Bathurst, 1971), sandstones (Heald, 1955; Baron and Parnell, 2007), and shales (Rutter, 1983). They appear as column-and-socket interdigitation features (Nenna and Aydin, 2011; Croizé et al., 2013) and are filled with insoluble elements such as organic matter, oxides, or clay particles (Nelson, 1981). Stylolites grow orthogonal to the major principal stress and are often divided in two groups: sedimentary stylolites oriented subparallel to bedding (i.e., those that form due to overburden stresses) and tectonic stylolites (perpendicular or oblique to bedding).

Stylolites have interested geoscientists for now almost a century primarily because, as compaction localization features, they could potentially impact fluid flow at various scales. Until recently, prevalent views on this matter were that stylolites were barriers to fluid flow (see for example Dunnington, 1967). Recent experimental studies revealed however that stylolites in limestones do not influence permeability when they are oriented perpendicular to fluid flow and, in some cases, can act as conduits when orientated parallel to flow (Lind et al., 1994; Heap et al., 2014a; Rustichelli et al., 2015). In the last decade, several studies also used stylolites as palaeostress gauges by linking their morphology to in situ stresses (e.g., Schmittbuhl et al., 2004; Rolland et al., 2012).

In situations where stylolites are abundant, another outstanding question important for reservoir/aquifer production (and a wide variety of geotechnical applications) is their impact on the mechanical strength and rheology of sedimentary formations. This question has received less attention from the scientific community perhaps because its answer appeared somehow obvious. The prevalent views are that the presence of stylolites significantly weakens rocks (Yates and Chakrabarti, 1998; Larbi, 2003; Özvan et al., 2011), that stylolites are natural planes of weakness in sedimentary formations (Nicholson and Nicholson, 2000; Pires et al., 2010), and that they induce a significant mechanical anisotropy (Rashed and Sediek, 1997). The fact that stylolites weaken a rock mass is supported by many observations in quarries. López-Buendía et al. (2013), for example, noted that more than 95% of cm-scale breakages within the quarried Crema Marfil marble (Alicante, Spain) were due to stylolites. Although very low strength was reported in Brazilian tests on the same material with open stylolites (López-Buendía et al., 2013), no study has, to our knowledge, systematically quantified the impact of stylolites on rock strength. One reason is probably that, in both field and laboratory contexts, the opening of the stylolites due to drilling, cutting, or depressurization, is a major issue and there is always some ambiguity whether the observed effect could in fact not primarily be due to some significant microcracking/fracturing associated to the stylolites and not to the structure itself. To what extent are stylolites planes of weakness if they are not open? Do they induce any mechanical anisotropy in that case, and is it possible to systematically quantify the weakening, if it exists at all? To answer these questions we performed a series of uniaxial compression tests on samples prepared from cores

* Corresponding author.

http://dx.doi.org/10.1016/j.tecto.2016.03.004
0040-1951/

taken from a borehole drilled in a limestone formation in the Paris Basin (France). Stylolites are abundant in this formation and Heap et al. (2014a) recently showed that it is possible to prepare samples in various orientations without opening the stylolites. We were therefore able to systematically compare the mechanical behaviour of these limestones with and without stylolites. Guided by new petrophysical measurements and microstructural observations, numerical modelling was used to interpret our mechanical data and clarify the role of stylolites on the brittle strength of carbonate rocks.

2. Material studied and experimental set-up

2.1. Material origin and preparation of the samples

In this study, we focused on Oxfordian limestones from the Eastern part of the Paris Basin. Several boreholes were drilled surrounding the Andra (French national radioactive waste management agency) Underground Research Laboratory (URL) near Bure, France. All the limestones studied here are allochemical (oolitic) limestones. They are all from the same borehole and belong to units located above the URL, which is built within a layer of claystone (see Rolland et al., 2014 for details). Stylolites are abundant in most of the retrieved cores (Fig. 1A). The larger stylolites (of cm thickness) were open in all cases, probably due to the depressurization upon retrieval. It is important to specify that the thickness to which we refer to in this study is the actual thickness of insoluble elements that can be seen by eye. For this study, we focused on sedimentary stylolites and selected zones presenting regularly spaced closed stylolites surrounded by sufficient reference stylolite-free material to be used for comparison. The typical distance between the studied stylolite and the stylolite-free material was about 10 cm. We avoided zones with large heterogeneities, anostomosing stylolites, and stylolites with tilted teeth. We also disregarded partially open stylolites that we could easily spot from the high resolution pictures of Rolland (2013). Because of these quite restrictive criteria, we could not sample the available cores at regular interval of depths. We focused on 6 different depths between 158 and 364 m. The geological and textural details of these layers, named for simplicity in this study O1 to O6, are given in Table 1 (based on the previous systematic study of André (2003)). The studied units are grainstones, wackestones, and packstones. The stylolites in these different layers show different morphologies, studied in detail by Rolland et al. (2014). In particular, the amplitude of the teeth was observed to be quite variable, from ~1 mm (Fig. 1B) to ~1 cm and sometimes more (Fig. 1C).

Cylindrical samples nominally 4 cm long and 2 cm in diameter with and without stylolites were prepared from the 10 cm diameter cores (Fig. 2A–B). For the samples containing stylolites, two orientations were cored: orthogonal and parallel to the stylolite plane. For simplicity, we will refer to these samples henceforth as orientation Z (samples cored orthogonal to the stylolite plane and stress also applied orthogonal to the stylolite plane) and orientation X (samples cored parallel to the stylolite plane and stress also applied parallel to the stylolite plane), respectively. Where possible, several samples at an oblique orientation (~60° to the core axis) were also prepared (Fig. 2C). At each selected depth, stylolites with different morphologies were encountered (Rolland et al., 2014). We grouped the stylolites that showed common morphological attributes and when possible obtained all the data from the same stylolite. This preparation phase was challenging and coring in three different orientations often minimized the number of cores we could prepare from a given length of core. Further, cutting and drilling into the cores occasionally revealed large heterogeneities, local

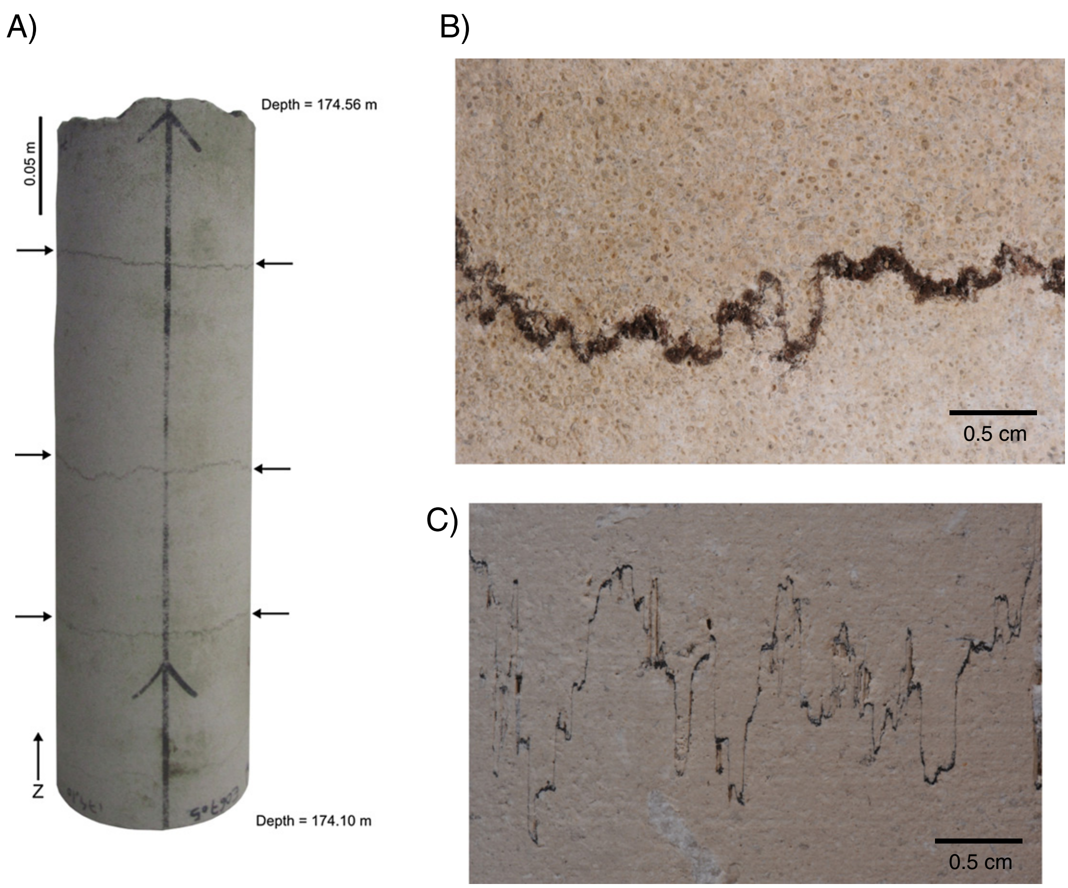

Fig. 1. (A) Photograph of a section of a core from the borehole EST205 from the ANDRA site in Bure, France. Three stylolites (indicated by arrows) are visible on the core of ~50 cm length. High resolution photographs showing the details of a stylolite in layers O3 (B) and O5 (C).

Table 1
Petrophysical description of the carbonates investigated in this study.

Rock sample code (Andra reference code)	Depth (m)	Average porosity (%)	Lithology
O1 (EST06683)	159	16.8	Packstone to wackestone
O2 (EST07755)	228	19.8	Grainstone to packstone
O3 (EST06705)	174	15.1	Grainstone
O4 (EST06770)	214	7.1	Grainstone
O5 (EST06950)	316	14.4	Packstone
O6 (EST07042)	364	6.9	Packstone

variations in stylolite orientation, teeth of very high amplitude (with respect to the sample size), and additional stylolites invisible from the surface of the cores. Additionally, some stylolites opened during the sample preparation process. In the end, more than 25% of the prepared samples had to be disregarded.

2.2. Experimental procedure

All samples were first dried in vacuum at 40 °C for a minimum of 48 h. In this study we performed "dry" (samples vacuumed at 40 °C for 48 h) and "wet" (samples vacuumed at 40 °C for 48 h and then vacuum-saturated in deionized water and left in the vacuum under water for 48 h) experiments. All the samples were deformed uniaxially until failure at a constant strain rate of 10^{-5}/s. Saturated samples were deformed in a water bath. We performed a total of 48 uniaxial tests, including 32 on samples containing a stylolite. More details about the experimental set-up can be found in Heap et al. (2014b). In a large majority of cases, the failure was unstable and the samples could not be retrieved for post-mortem microstructural analysis. However we managed to stop a few experiments before failure. Petrographic thin sections were prepared from these deformed samples.

3. Petrophysical and microstructural attributes of the studied carbonates

Systematic petrophysical and microstructural analysis over the whole length of the EST205 borehole was recently provided for the stylolite-free limestones by Regnet et al. (2015a), see in particular their Fig. 6. We refer the reader to this study for further details on the stylolite-free materials. In this section we will focus on the main microstructural attributes of the studied rocks and on the potential petrophysical differences induced by or associated to the presence of stylolites. Previous studies on the same carbonates revealed that these materials are composed of more than 97% calcite with minor percentages of dolomite, quartz, and clay (Heap et al., 2014a), also in agreement with Regnet et al. (2015a) who reported a composition >99% calcite in their samples from the same borehole. The studied limestones have another common attribute: they are all microporous (Heap et al., 2014a; Regnet et al., 2015a). Fig. 3A shows as an example a SEM photomicrograph of horizon O1 where the microporosity appears heterogeneously distributed. The larger pores visible in this image have a diameter of about 10–15 μm (Fig. 3B). All the studied carbonates have a high degree of cementation, as illustrated in horizon O3 (Fig. 3C). No pore larger than 5 μm could be observed in this layer. X-ray Computed Tomography (CT) data were also acquired at a resolution of 4 μm on a 4 mm diameter sample from the same depth (Fig. 4). Even at this high resolution, one cannot resolve individual pores and the porosity is typically concentrated around the allochems (darker zones in the CT image).

Considering the low percentages of secondary minerals, it is reasonable to estimate the porosity of the samples using simply their dry mass and considering 100% calcite (assuming a calcite density of 2.71 g/cm^3). We checked this assumption performing porosity measurements on a selection of samples using a helium pycnometer. We found in all cases

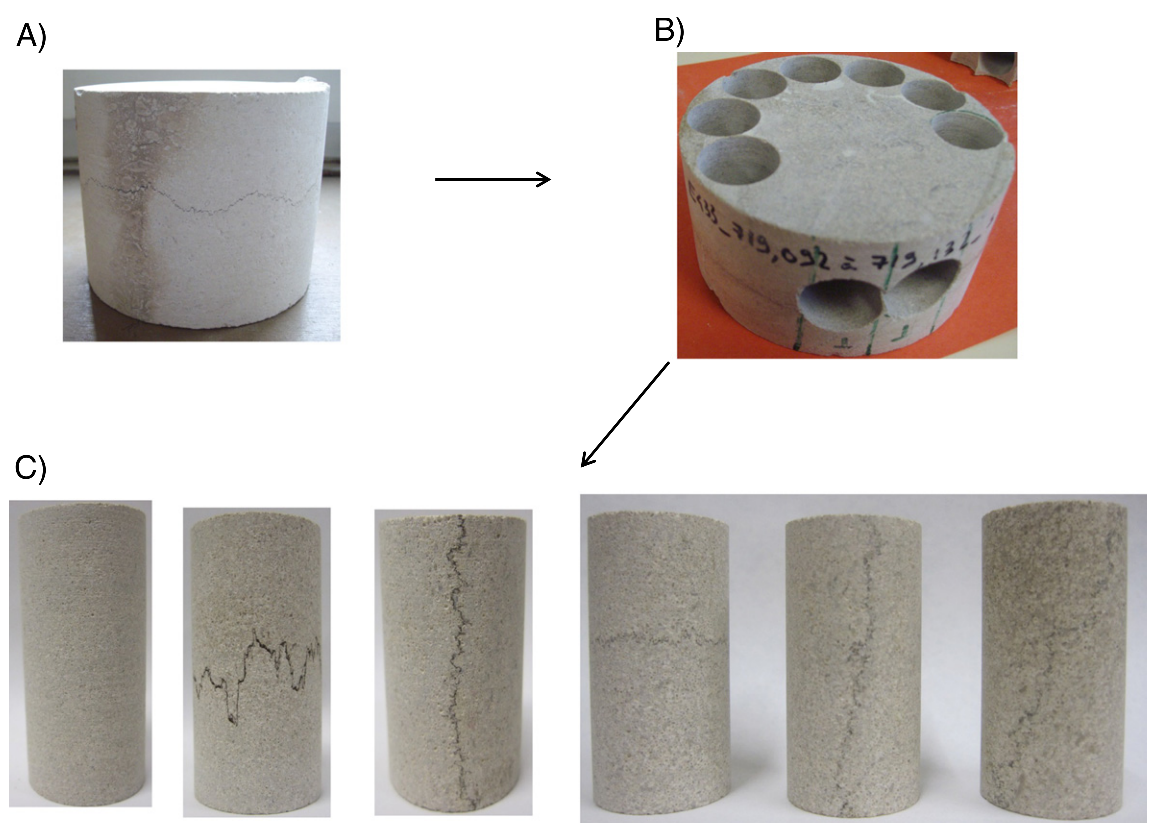

Fig. 2. Preparation of the samples with a stylolite. (A) Slices of about 10 cm were cut in the cores such that the stylolite is in the middle. (B) We cored in several orientations in this slice (B) to obtain samples with horizontal, vertical and oblique stylolite (C).

Please cite this article as: Baud, P., et al., Impact of stylolites on the mechanical strength of limestone, Tectonophysics (2016), http://dx.doi.org/10.1016/j.tecto.2016.03.004

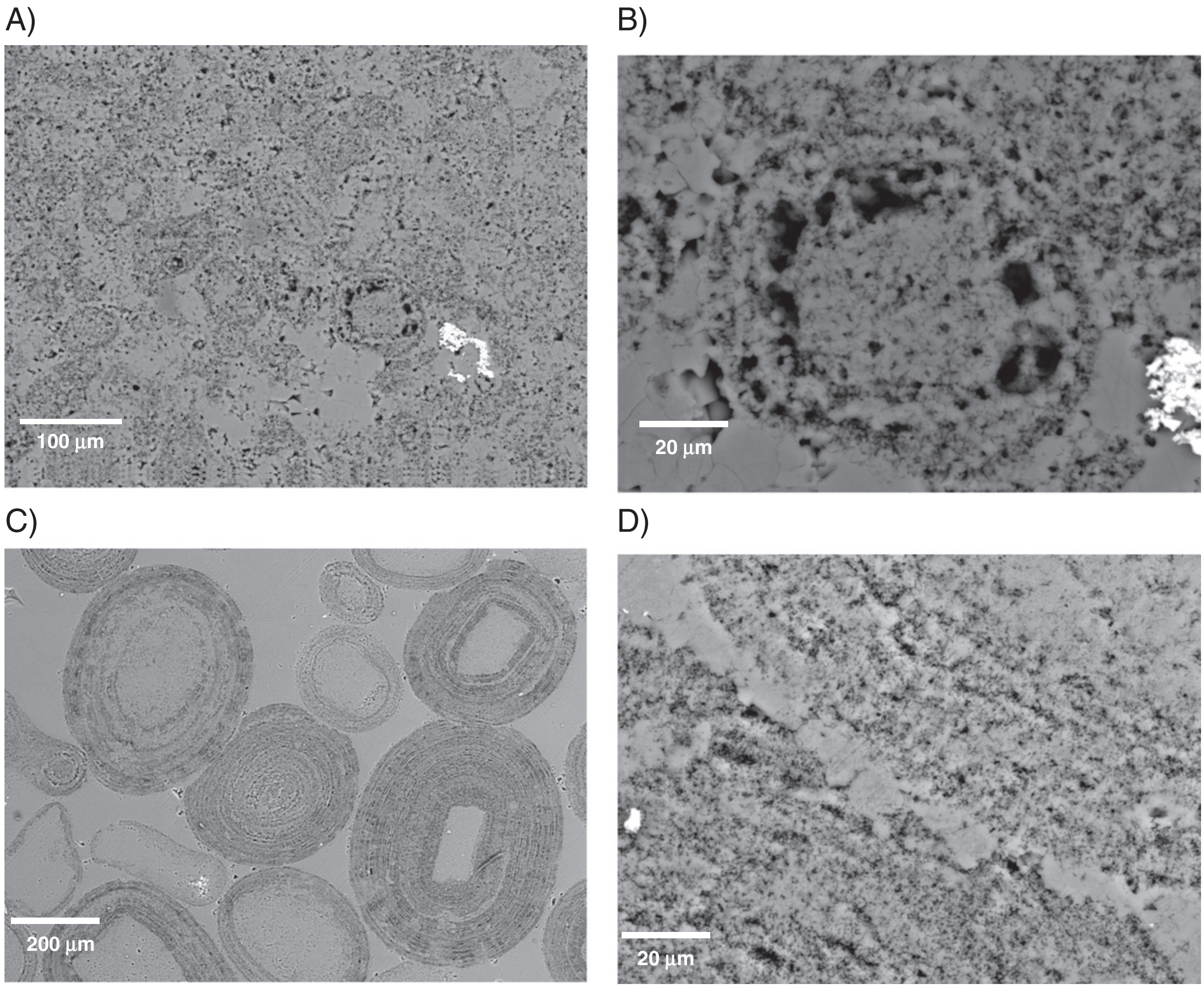

Fig. 3. SEM micrographs showing the microporous nature of the carbonates from Bure: microporosity (A) and maximum pore size ~10 μm (B) in an intact sample of layer O1. Highly cemented structure (C) and smaller pore size (D) in an intact sample of oolitic grainstone (layer O3). Porosity appears as black in the micrographs.

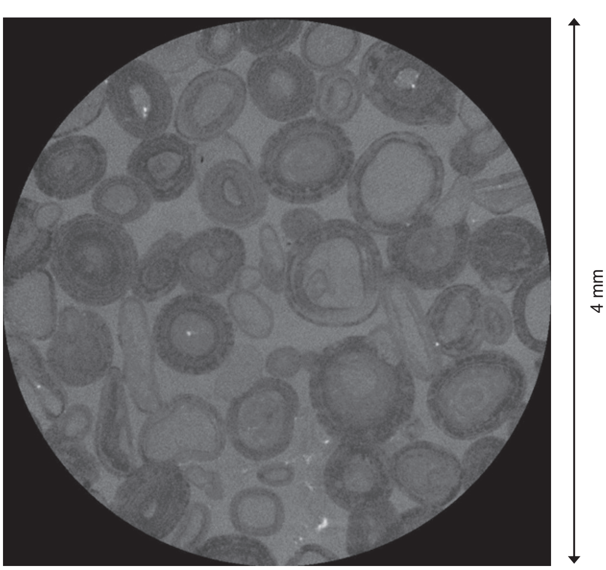

Fig. 4. Micro CT data with resolution 4 μm data on an intact sample of oolitic grainstone (layer O3). No macropores are visible and the microporosity appears to be greater close to the edge of the allochems (dark areas).

less than 5% of difference between the porosities measured with the pycnometer and those inferred from the dry mass. This also means that the proportion of disconnected porosity, if any exists, is within the error bars of the measurements. For the saturated samples, we observed a difference of about 0.01% (on average) between the porosity determined by triple weight and that determined by the dry mass only. It is likely that water failed to saturate all of the very small pores (<1 μm). However, while this imperfect saturation could be an issue for some petrophysical measurements, Schmitt et al. (1994) showed on various rock types that it has virtually no effect on the brittle strength for saturation as low as 20%.

The porosity of our samples was found in the range 0.06 to 0.21. The average porosity for the 6 layers is given in Table 1. We observed that sample porosity decreases with depth (Fig. 5). All the samples with a stylolite were found, independent of the orientation, to be more porous than the stylolite-free host rock and the measured difference in porosity was between 0.01 and 0.03. Higher porosities associated with the presence of stylolites were also reported in several previous studies (Dawson, 1988; Braithwaite, 1989; Raynaud and Carrio-Schaffhauser, 1992; Lind et al., 1994; Heap et al., 2014a, Rustichelli et al., 2015). This could be related to the formation of the stylolite, in particular if stylolites are seen as the product of the horizontal linkage and vertical coalescence of numerous pressure-solution seams (Nenna and Aydin, 2011), a scenario that promotes the development of secondary porosity.

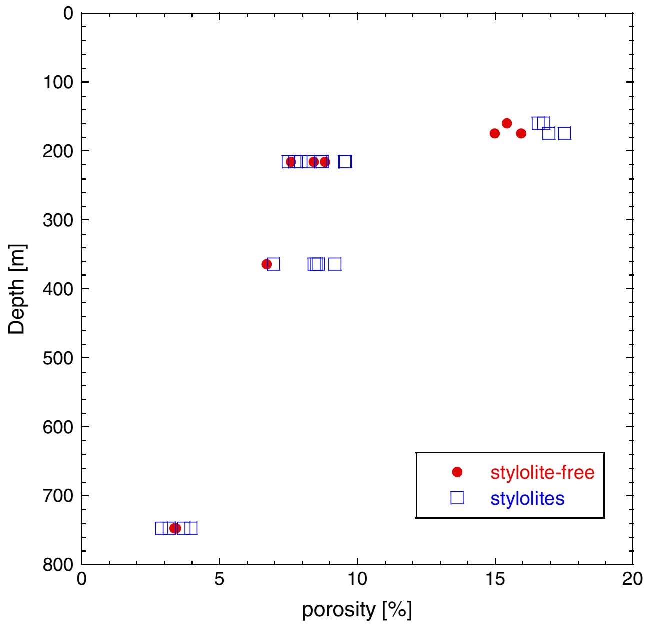

Fig. 5. Porosity of the carbonates from Bure as a function of depth: stylolite-free samples (red circles) and samples with a stylolite (blue squares). (For interpretation of the references to colour in this figure legend, the reader is referred to the web version of this article.)

High-porosity zones may also be due to vuggy porosity patches along stylolites (Rustichelli et al., 2015). Other interpretations of these higher porosity zones could be the injection of non-equilibrated fluid if stylolites acted as conduits for flow, or more simply the fact that the stylolites grew preferentially in zones of higher porosity, as suggested for the formation of compaction bands (Vajdova et al., 2012, Cilona et al., 2012, 2014).

We estimated the extent of the higher porosity zone surrounding the stylolites by making porosity measurements at regular intervals (~0.5–1 cm) on several cylindrical columns of 10 cm length. A representative example for the horizon O3 is shown in Fig. 6A. One can see that significantly higher porosity was only observed adjacent to the stylolite (up to a distance of 0.5 cm). This means that for a 4 cm length sample cored perpendicular to bedding, as shown in Fig. 2, there will be a significant difference in porosity between the central part of the sample and the sample ends. Mercury injection experiments at pore pressures up to 413 MPa were also performed on a few selected samples taken from the same column (Fig. 6B). Most of the pore-throats have a diameter < 1 μm. These data also suggest that the average pore-throat diameter increased slightly as the stylolite was approached.

Rolland (2013) presented some P-wave velocity data and specific area measurements on the same carbonate layers. These data did not reveal any systematic variations in the vicinity of the stylolite. This confirmed our visual and microstructural observations that the higher porosities measured close to the stylolite were not due to microcracking.

Previous studies on stylolites also stressed that they are expected to have a complex internal structure due to the hierarchical nature of their formation, combined with the impact of grain-scale heterogeneities (Ebner et al., 2010) and to the inhomogeneous stress distribution surrounding geometric asperities (Zhou and Aydin, 2010). The first order consequence of this complexity is that the stylolite and its surroundings are also more heterogeneous than the host rock. Fig. 7A shows the tortuous path of a stylolite in layer O3. While the stylolites are clearly visible on the sample surface, they are more challenging to follow at smaller scale (i.e., under the microscope). It is their complex and heterogeneous nature, containing partially dissolved grains (Fig. 7b), which allow us to follow their trace in optical and SEM micrographs.

4. Mechanical data

Representative stress–strain curves are presented in Fig. 8. For reasons explained earlier, we had to disregard a fair number of samples and this is why we cannot provide a complete set of dry and wet experiments for all the orientations and all the layers. When we anticipated

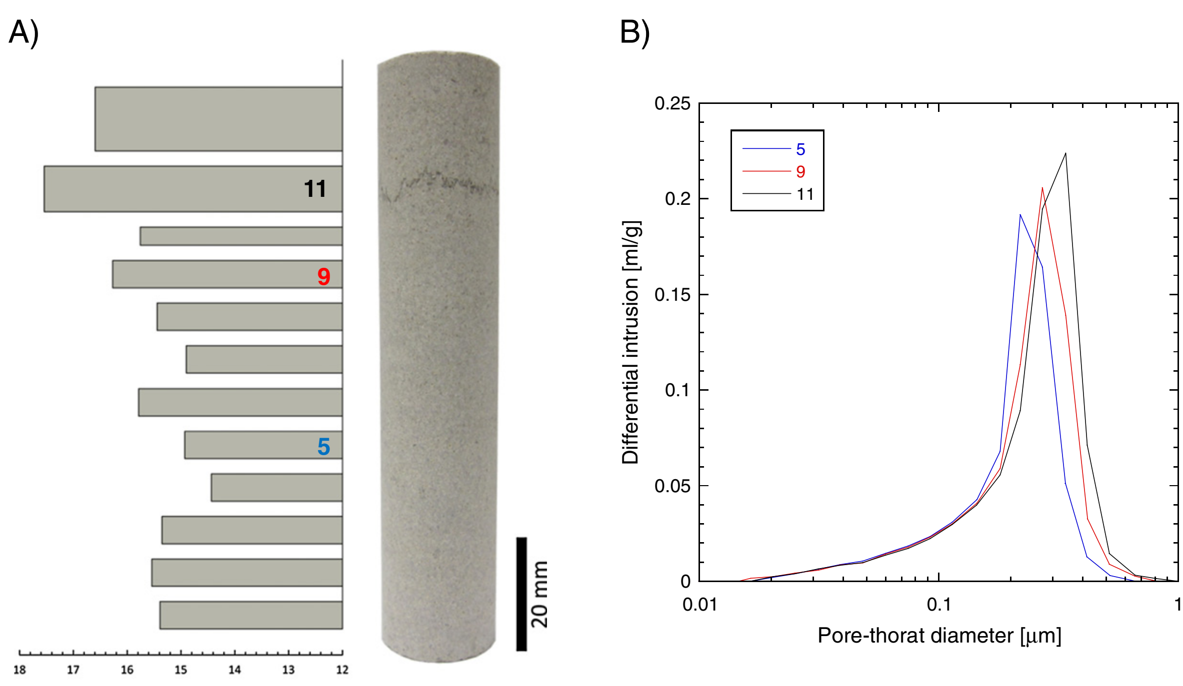

Fig. 6. (A) Evolution of the porosity of the layer O3 near a stylolite. (B) Mercury injection data for the samples 5 (blue), 9 (red) and 11 (black) of the same column: Differential intrusion as a function of pore-throat diameter. (For interpretation of the references to colour in this figure legend, the reader is referred to the web version of this article.)

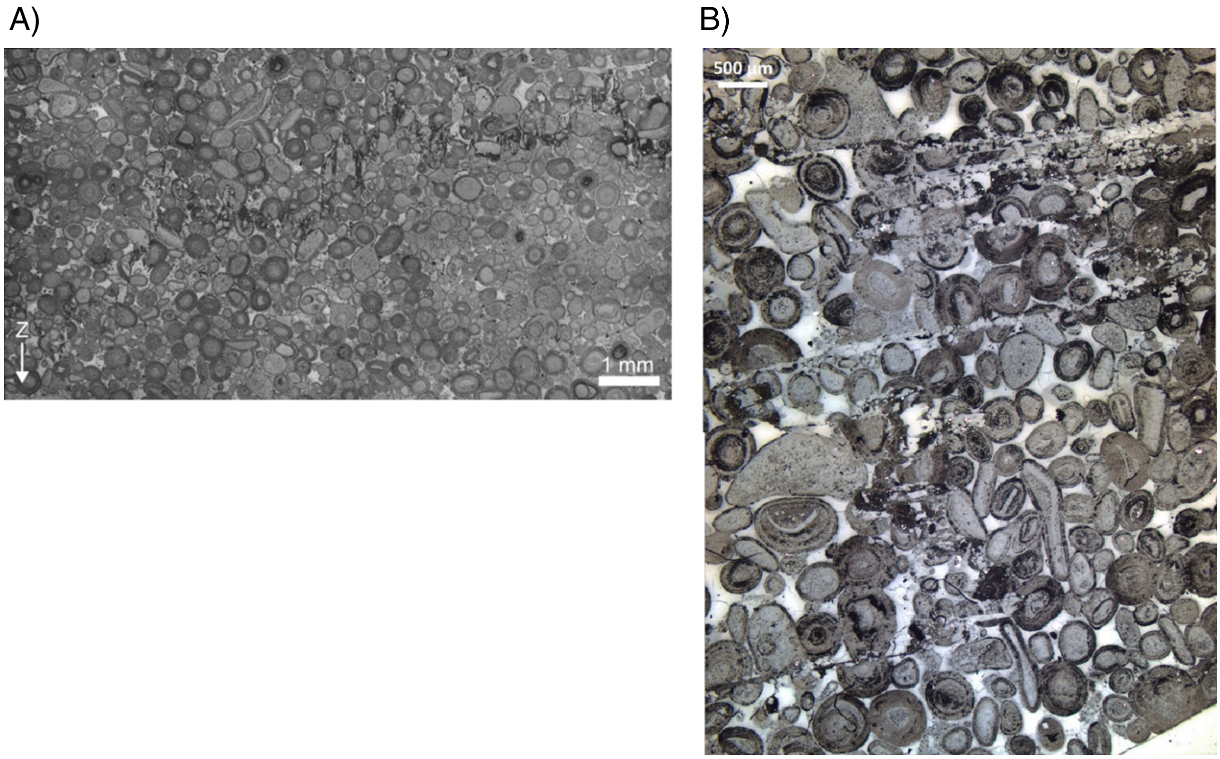

Fig. 7. (A) Mosaic of optical micrographs (cross-polarized light) showing a stylolite. (B) Mosaic of SEM micrograph showing the details of a stylolite in layer O3.

that testing all the orientations would not be possible, we used the remaining parts of the cores to duplicate certain tests and appreciate the repeatability of the results.

We observed that the Uniaxial Compressive Strength (UCS) of the stylolite-free limestone is in the range 48–150 MPa in dry conditions and 30–90 MPa in wet conditions. The stylolite-free material did not show any evidence of mechanical anisotropy, as shown on Fig. 8F for layer O3. This is perhaps not unexpected since Rolland (2013) and Heap et al. (2014a) did not measure any P-wave velocity or permeability anisotropy on the same rocks, respectively.

As far as the impact of stylolites is concerned, the main features that can be seen in Fig. 8 are the following:

- The stress–strain curves of the stylolite-bearing samples and the stylolite-free samples did not show any significant differences, and both were typical of what is usually observed in this type of uniaxial experiment: after an elastic (quasi-linear) stage, the curves reached a peak beyond which strain softening and unstable failure occurred. We note however that the failure appeared more unstable when the stylolite was oriented parallel to the applied stress.
- All the stylolite-bearing samples are weaker than the corresponding stylolite-free samples.
- The difference in strength between the stylolite-bearing samples and the stylolite-free samples is about the same under dry and wet conditions.
- In all tested horizons, the presence of a stylolite did not induce any mechanical anisotropy and the UCS was about the same for samples with a stylolite oriented orthogonal, parallel, or oblique to the direction of the applied stress (vertical).
- In most cases, the tangent modulus of the stylolite-bearing samples was smaller than that of the stylolite-free samples.

5. Failure modes and microstructural observations

All the stylolite-free samples failed by axial splitting (Fig. 9A). We managed to stop one of the experiments on layer O3 shortly after the peak stress. As expected, we observed homogeneously-distributed axial microcracking in the sample; the microcracks cut through both the cement and the ooids (Fig. 9B). The failure mode was similar (axial splitting) for samples with a stylolite oriented orthogonal to the applied stress. Even though our experimental set-up allowed us to observe the sample during deformation, it was not always possible to spot from where the main fracture initiated. Post-mortem observations of these samples showed that the main macroscopic fracture either cuts through the stylolite plane (Fig. 9C), or that it occurred in two stages where half of the sample is first broken from one end to the stylolite plane, and then the failure continued seconds later from the same position in the stylolite plane or with some horizontal offset as in the example shown in Fig. 9D. We studied the microstructure of one deformed sample of layer O5 that showed less obvious damage. An SEM micrograph of this sample (Fig. 9E) revealed that part of the axial microcracking initiated from the stylolite plane and in particular from the larger teeth of the stylolite. These observations suggest that, in this orientation, the stylolite plane (and perhaps its surroundings) acted as a zone of high stress concentration and played a fundamental role in the development of stress-induced damage the and failure of the sample.

When the stylolite plane was oriented parallel or oblique with respect to the applied stress, we observed different failure patterns in

Fig. 8. Representative mechanical data for uniaxial compression tests performed on carbonates from Bure. Axial stress is presented as a function of axial strain for experiments performed on stylolite free samples (plain lines) and samples with a stylolite (dashed lines). Samples cored orthogonal (Z), parallel (X) and oblique to bedding are presented in blue, red and green, respectively. For samples with a stylolite, triangles indicate the orientation of the stylolite. Dry data are presented on layers O1 (A), O6 (B), O2 (C), O3 (E), and O5 (G) and wet data on layers O1 (B), O2 (D), O3 (F), and O5 (H).

Please cite this article as: Baud, P., et al., Impact of stylolites on the mechanical strength of limestone, Tectonophysics (2016), http://dx.doi.org/10.1016/j.tecto.2016.03.004

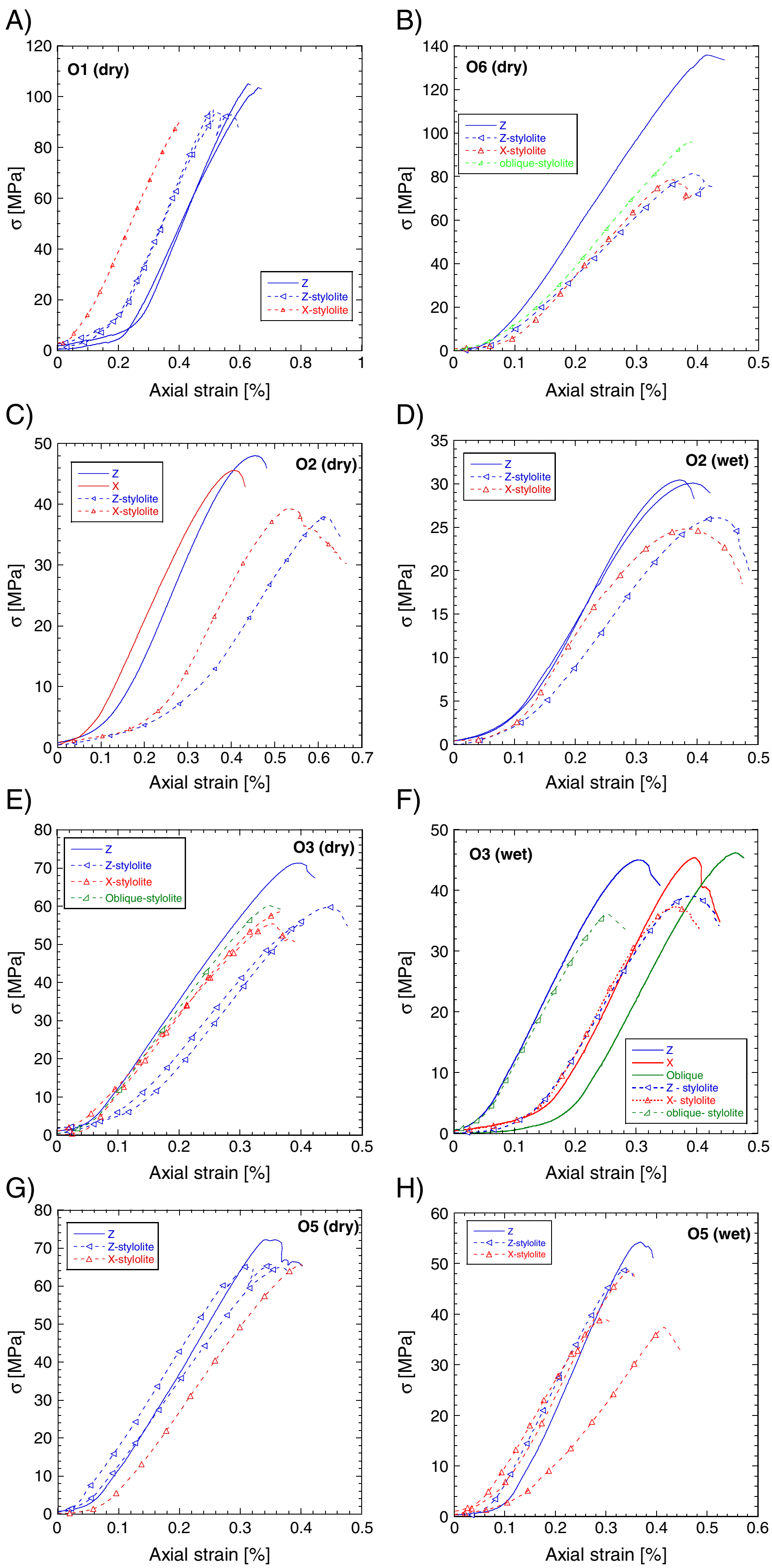
A)
O1 (dry)
Z
Z-stylolite
X-stylolite
σ [MPa]
Axial strain [%]
B)
O6 (dry)
Z
Z-stylolite
X-stylolite
oblique-stylolite
σ [MPa]
Axial strain [%]
C)
O2 (dry)
Z
X
Z-stylolite
X-stylolite
σ [MPa]
Axial strain [%]
D)
O2 (wet)
Z
Z-stylolite
X-stylolite
σ [MPa]
Axial strain [%]
E)
O3 (dry)
Z
Z-stylolite
X-stylolite
Oblique-stylolite
σ [MPa]
Axial strain [%]
F)
O3 (wet)
Z
X
Oblique
Z - stylolite
X- stylolite
oblique- stylolite
σ [MPa]
Axial strain [%]
G)
O5 (dry)
Z
Z-stylolite
X-stylolite
σ [MPa]
Axial strain [%]
H)
O5 (wet)
Z
Z-stylolite
X-stylolite
σ [MPa]
Axial strain [%]

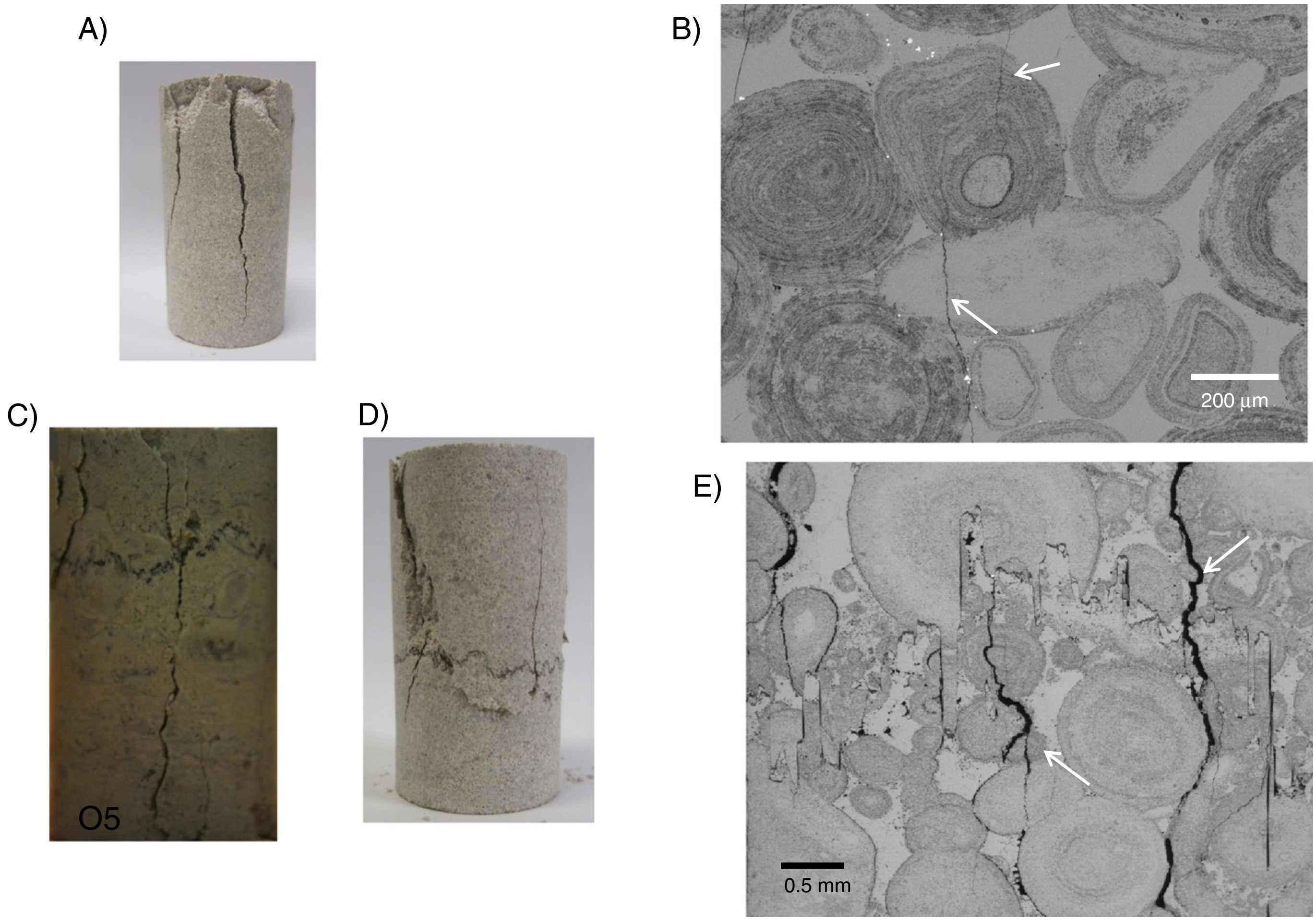

Fig. 9. (A) Photograph of a stylolite-free sample of layer O3 deformed uniaxially under nominally dry conditions and which failed by axial splitting. (B) SEM micrograph of a sample of layer O3 deformed uniaxially just beyond the peak stress: axial microcracks (indicated by white the arrows) cut through the cement and the oolites. Photographs of deformed samples with a horizontal stylolite (orientation Z): (C) from the layer O5 with axial microcracking cutting through the stylolite and (D) from layer O3 showing a more complex failure mode. (E) SEM micrograph of a sample from layer O5 deformed to the peak stress showing that microcracking (indicated by the white arrows) initiated from some of the larger teeth of the stylolite. Uniaxial stress was applied in the vertical direction.

the different samples. The common attribute was the fact that failure occurred sub-vertically in most samples and some damage was always associated to the stylolite plane. This could be easily verified on the broken samples since the fracture plane appeared dark when it followed the stylolite plane (cutting through the insoluble layer) and white when the fracture developed outside the stylolite plane. When the stylolite was oriented parallel to the applied stress, visual inspection of the broken samples suggested that the main failure was in all cases strongly influenced by the presence of the stylolite (Fig. 10). When the stylolite was very tortuous, macroscopic cracking cut sub-vertically through its larger (horizontal) teeth, as in the example shown in Fig. 10A. When the stylolite was less tortuous, we often observed only a partial overlap between the stylolite and the failure plane (Fig. 10B), probably due to end effects and/or to the presence of heterogeneities in the sample. We also observed in some cases that failure developed quasi-simultaneously in and outside the stylolite plane (Fig. 10C). Fig. 10D–E shows SEM micrographs from a sample of O5 that was unloaded just after the peak stress. The density of axial microcracks appeared larger in the vicinity of the stylolite. In some cases, sub-vertical microcracks followed the stylolite path (Fig. 10D) and sometimes cut through the larger teeth when the stylolite became more tortuous (Fig. 10E).

We had only a few samples with oblique stylolites because their preparation limited considerably the number of available samples in the other orientations from the same stylolite. In the deformed samples with an oblique stylolite, we observed that macroscopic failure occurred for the most part on the stylolite plane, as in the example shown in Fig. 11A. In this orientation, the failure mode was therefore different from the axial splitting seen in other orientations. However, we also typically observed some axial microcracking emanating from the stylolite, creating secondary sub-axial macrofractures (Fig. 11A). SEM microstructural observations made on a sample of deformed O5 just beyond the peak stress confirmed what visual inspection of the samples suggested: when the stylolite was less tortuous, stress-induced damage mostly followed its path (Fig. 11B). However, when the stylolite was more tortuous, including some sub-horizontal segments, stress-induced microcracks were mostly observed in the direction of the applied stress (Fig. 11C).

In summary, in all deformed samples with a stylolite, visual inspection and microstructural observations suggested a major influence of the stylolite on stress-induced damage and failure, consistent with our mechanical data showing that the presence of a stylolite always induced weakening (Fig. 8).

6. Stochastic modelling

The analysis of brittle failure in stylolite-bearing samples could not be achieved using standard micromechanical modelling (see for example Baud et al., 2014) due to the inherent heterogeneity of these samples (see Section 3). One has to therefore rely on numerical modelling for

Please cite this article as: Baud, P., et al., Impact of stylolites on the mechanical strength of limestone, Tectonophysics (2016), http://dx.doi.org/10.1016/j.tecto.2016.03.004

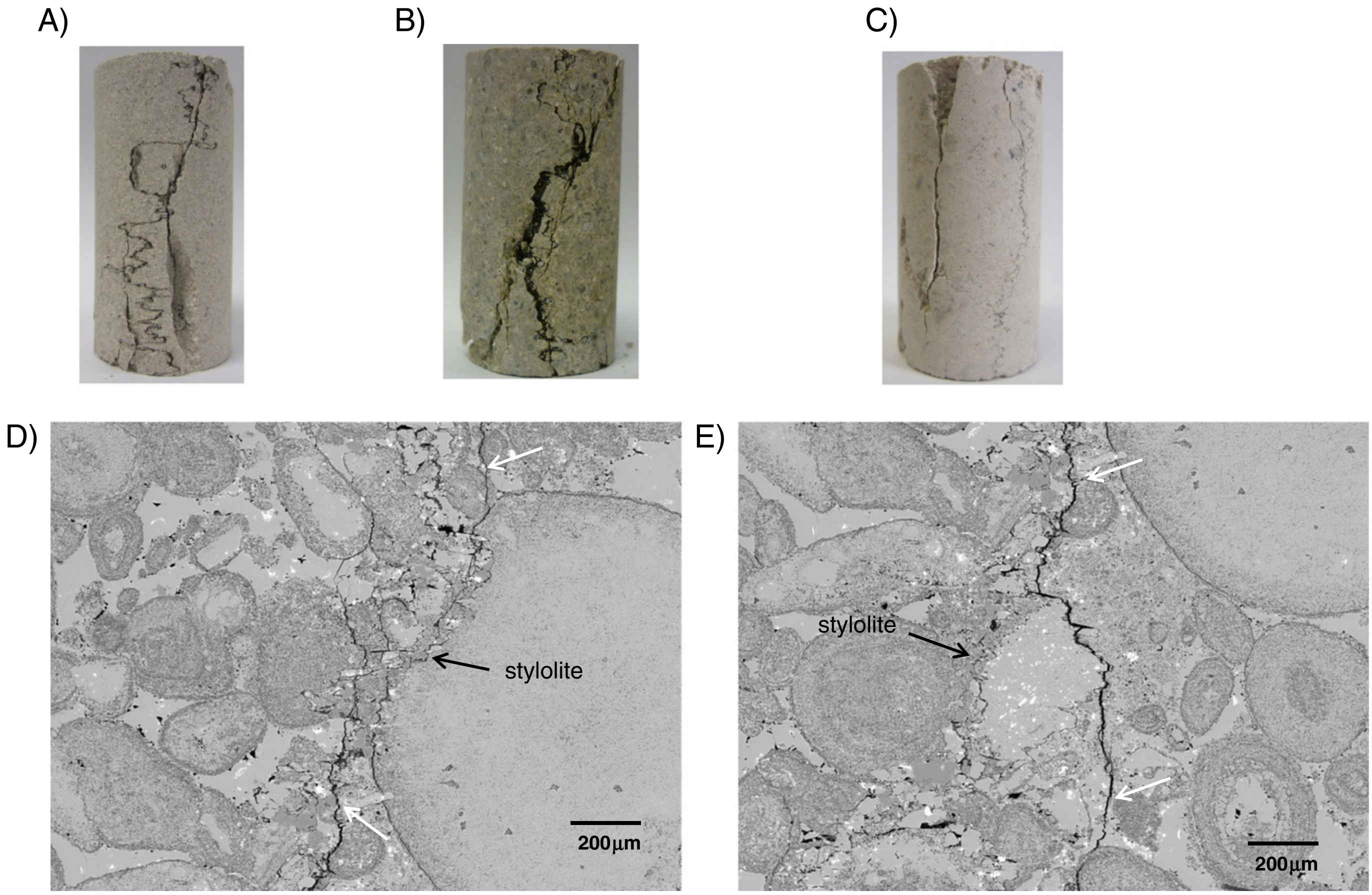

Fig. 10. Photographs of deformed samples with vertical stylolite (orientation X) from layers O3 (A–B) and O5 (C). SEM micrographs of sample of O5 deformed just beyond the peak stress: axial microcracking (indicated by the white arrows) following the stylolite (D) and close to the stylolite in a more tortuous zone (E). Uniaxial stress was applied in the vertical direction.

this type of complex problem. In this study, we chose to use the 2D Rock Failure Process Analysis finite element code ($RFPA_{2D}$) developed by Tang (1997) and applied in several previous studies to brittle failure of carbonates (Wong et al., 2006) and, more recently, volcanic rocks (Heap et al., 2014c). The numerical samples of this study (rectangles 40 mm in length and 20 mm in width, the same size as the experimental samples) consist of 51,200 square elements (Fig. 12A). Because our carbonates are all microporous, we did not include any macroscopic voids in the numerical samples and assumed that the local strength of the element reflects the presence of micropores. To also reflect material heterogeneity at the element scale, each square is assigned Young's modulus and strength using a Weibull probability distribution function (Weibull, 1951):

$$f(\sigma) = \frac{m}{\sigma_0}\left(\frac{\sigma}{\sigma_0}\right)^{m-1} \exp\left[-\left(\frac{\sigma}{\sigma_0}\right)^m\right] \quad (1)$$

The statistics for failure involve therefore two parameters: σ_0 proportional to the mean of the strength distribution and m which characterizes the degree of heterogeneity of the material. High values of m lead to homogeneous samples, and vice-versa. Linear constitutive laws are considered for each element until failure that can occur in shear and tensile mode. Importantly, when an element fails, it is replaced by the same element with a considerably lower strength and Young's modulus. Further details on the model can be found in Tang (1997), Wong et al. (2006), and Xu et al. (2012).

We decided to apply this approach to our data on layer O3. The first step was to set the model parameters to match our mechanical data on the stylolite-free material. Table 2 presents the parameters used for this simple case and Fig. 13A shows the simulated stress–strain curve together with the experimental data. The evolution of damage (AE events) in this simple case is also shown in Fig. 13B. It is clear that the set of parameters required to produce such results is by no means unique, but this is of little importance in this study since we primarily focused here on the impact of stylolites.

In Fig. 13B, each circle symbol represents one AE event corresponding to the failure of one element in the numerical sample. The size of the circle represents the magnitude of the released energy and the colour represents the type of event (white = shear crack induced by a compressive stress and red = tensile crack induced by tensile stress). A black circle represents a failed element or an AE event in a former calculating step.

The second step was to create numerical samples representative of the samples with a stylolite in the different orientations. Guided by our petrophysical data, we first examined the possibility that the observed mechanical behaviour and damage patterns would be mostly due to the fact that the thin stylolite is in the middle of a weaker, more porous zone. We therefore performed a first series of simulations with the geometries shown in Fig. 12C–D. The presence of the stylolite in the samples was modelled as a 5 mm-thick zone, while the rest of the sample was assigned the same properties than the stylolite-free sample. Numerous attempts were made using these geometries in which we varied the thickness and properties of the "stylolite zone" to yield results comparable to our mechanical data on layer O3. Of course, the geometries shown in Fig. 12C–D introduced more parameters in the model, but the models containing a stylolite were better-constrained using the measured values of strength and elastic parameters in three

Please cite this article as: Baud, P., et al., Impact of stylolites on the mechanical strength of limestone, Tectonophysics (2016), http://dx.doi.org/10.1016/j.tecto.2016.03.004

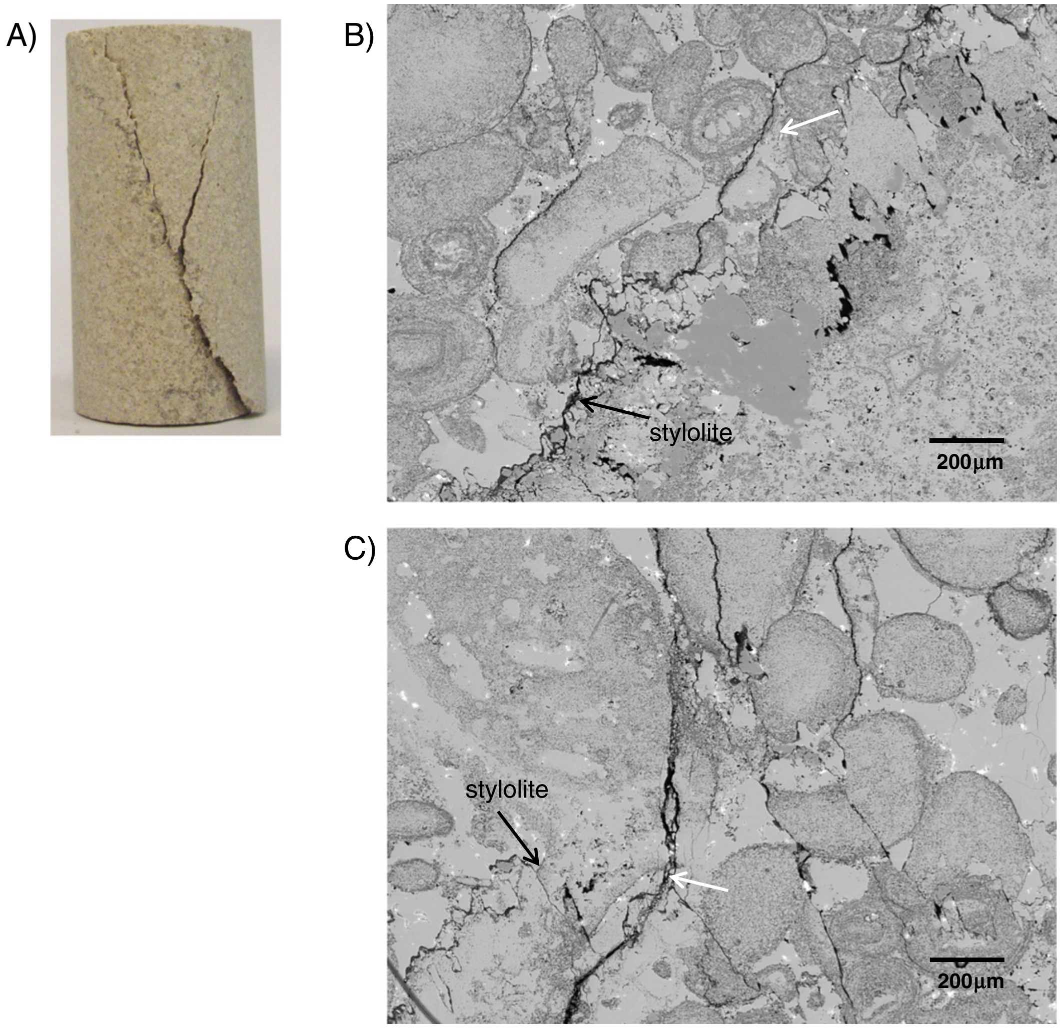

Fig. 11. (A) Photograph of a deformed sample of O3 with an oblique stylolite. Failure occurred both in and out of the stylolite plane. SEM micrographs of a sample of O5 with an oblique stylolite deformed just beyond the peak stress: (B) Microcracking (indicated by the white arrow) following the stylolite, (C) sub-axial microcracking (indicated by the white arrows) initiating from a sub-horizontal part of the stylolite. Uniaxial stress was applied in the vertical direction.

orientations. Our parametric study showed that our uniaxial data on layer O3 could be reasonably approached if one considers that the strength of the stylolite zone is 10% less than that of the stylolite-free sample. The parameters for this case, which we will call Simulation 1 from hereon in, are shown in Table 2. The simulated stress–strain curves and damage evolutions are shown in Fig. 14. Damage development in the simulation when the stylolite is either orthogonal or parallel to the applied stress is very similar to our post-mortem observations on the deformed samples (Fig. 14B and C). However, we noted two important discrepancies between the results of Simulation 1 and the experimental data. First, the model always predicted a mild mechanical anisotropy (Fig. 14A) with the oblique orientation always significantly weaker, in contrast to our data. Second, and clearly related to the previous point, failure in the oblique orientation is predicted to occur solely in the stylolite zone with little damage developing in the rest of the sample (Fig. 14D). Additional simulations with the same geometries, considering a more heterogeneous stylolite zone (decreasing *m* by 25%) and the same average strength as the stylolite-free material, led to results almost identical to those presented in Fig. 14. The conclusion is that the numerical samples considered in Fig. 12C–D are too simple, and the simulations suggest that the stylolite geometry needs to be considered in the simulations.

To check this, we implemented a second series of simulations (Simulations 2) on the numerical samples shown in Fig. 12E–G. This time, we digitized one of the stylolites observed in a sample containing a vertical stylolite and simply rotated this stylolite to create numerical samples containing stylolites in the other orientations. We imposed, as in Simulation 1, that the stylolite had the same properties as the stylolite-free material, except that its strength was 25% less (Table 2). These geometries did not result in any mechanical anisotropy and the simulated damage patterns are in qualitative agreement with our observations (Fig. 15B–D). In particular, the failure mode for the oblique stylolite was significantly different than in Simulation 1 due to the stylolite roughness, and failure occurred this time only partially on the stylolite plane (Fig. 15B). Similar to Simulation 1, when the average strength was the same for the stylolite and the stylolite-free material, qualitatively similar results were obtained when we made the stylolite more heterogeneous. Obviously a weaker and more heterogeneous stylolite with slightly different parameter combinations would also give similar results.

In summary, our numerical simulations using the $RFPA_{2D}$ code showed that it is possible to produce results in qualitative and quantitative agreement with our mechanical data and post-mortem observations by considering the following ingredients in the simulations:

-a stylolite seen as a weaker and/or more heterogeneous zone in a carbonate formation, in agreement with our petrophysical measurements and microstructural observations;

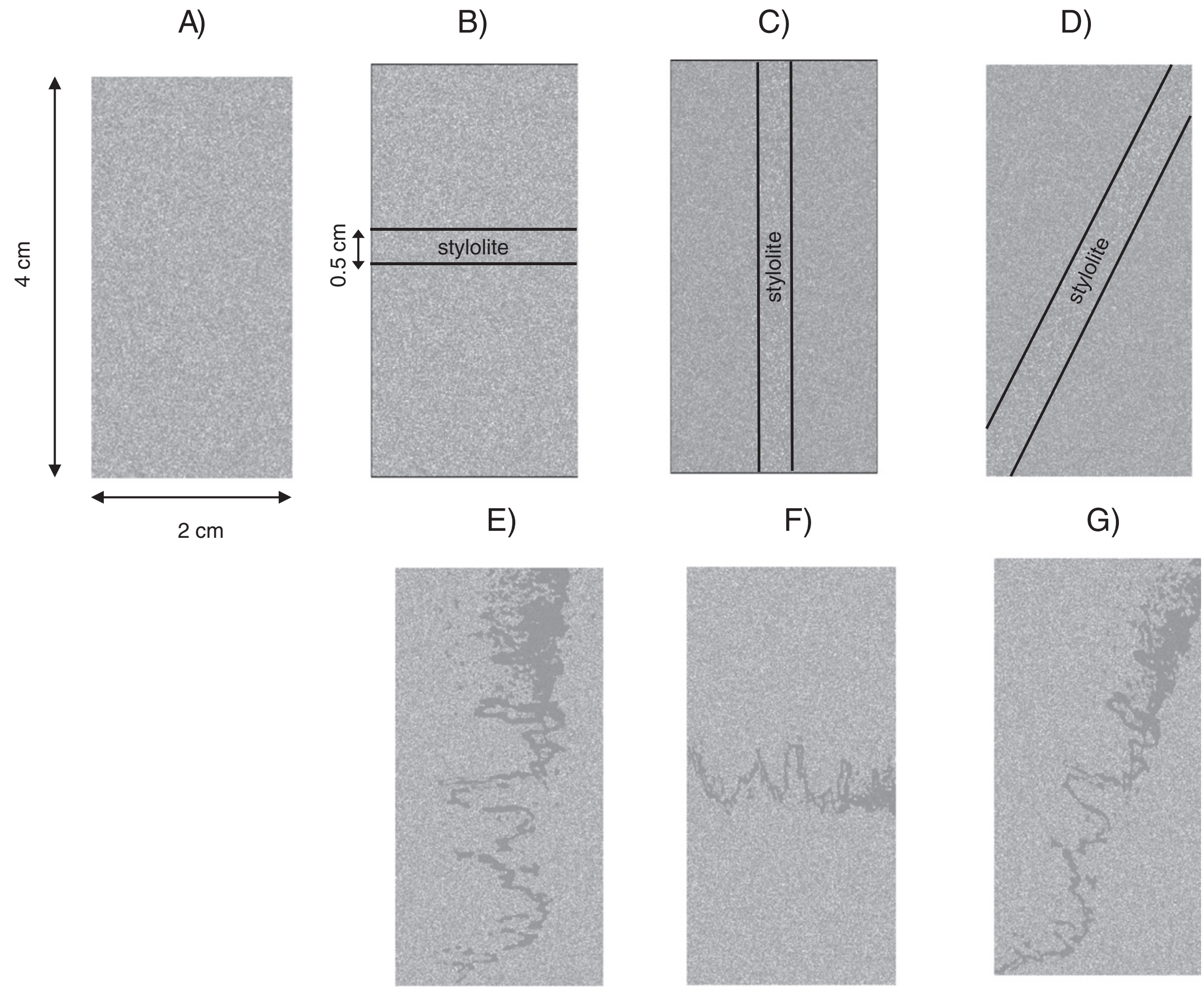

Fig. 12. Numerical samples used in the simulations performed with the RPFA code of Tang (1997). (A) Stylolite-free samples, (B–D) samples used for Simulation 1 with a 10% weaker stylolite zone, (E–F) samples used for Simulation 2 with a thin tortuous and 10% weaker stylolite.

-and a certain stylolite roughness which, according to the simulations, is the main factor leading to the absence of mechanical anisotropy.

7. Discussion

7.1. Microstructural control of mechanical strength of the limestone from Bure

We performed 16 uniaxial compression experiments on stylolite-free samples of limestone from Bure. We present in Fig. 16 our new dry UCS data against porosity for these samples, together with a compilation of data for allochemical and micritic limestones coming various locations from Zhu et al. (2010). We first note that the strength of the carbonates from Bure is in most cases between the compiled data for the allochemical and micritic limestones. This is not unexpected because, if the rocks from Bure are of allochemical origin, they showed a very high degree of cementation and a very small amount (or a total absence) of macropores, see Figs. 3 and 4 and the previous microstructural observations of Heap et al. (2014a) and Regnet et al. (2015a). This is in contrast to most allochemical limestones compiled in Fig. 16 (see for example the statistics on macroporosity recently presented in Ji et al., 2012 and 2015). Previous microstructural studies showed that the main micromechanism leading to brittle failure in porous limestone is pore-emanated microcracking (see for example Vajdova et al., 2010; Vajdova et al., 2012). This scenario was captured by Sammis and Ashby's (1986) micromechanical model. In this approach, spherical pores of constant radius are distributed homogeneously in the sample. When loaded beyond a certain stress, microcracks start to develop from the pores, eventually leading to macroscopic failure. Zhu et al. (2010) proposed a polynomial approximation of Sammis and Ashby's (1986) model for the uniaxial compression case which leads to the following simple expression for the UCS:

$$UCS = \frac{1.325}{\phi^{0.414}} \frac{K_{IC}}{\sqrt{\pi r}} \tag{2}$$

where ϕ is the porosity, r the pore radius, and K_{IC} the toughness of the material. Since the rocks studied here are carbonates, we take

Table 2
Physico-mechanical parameters of the numerical model.

Simulations	Homogeneity index	Mean compressive strength (MPa)	Poisson's ratio	Friction angle (°)	Coefficient from UCS to UTS
Styolite-free	2	240	0.25	30	10
Simulation 1					
Host rock	2	240	0.25	30	10
Stylolite zone	2	216	0.25	30	10
Simulation 2					
Host rock	2	240	0.25	30	10
Stylolite	2	216	0.25	30	10

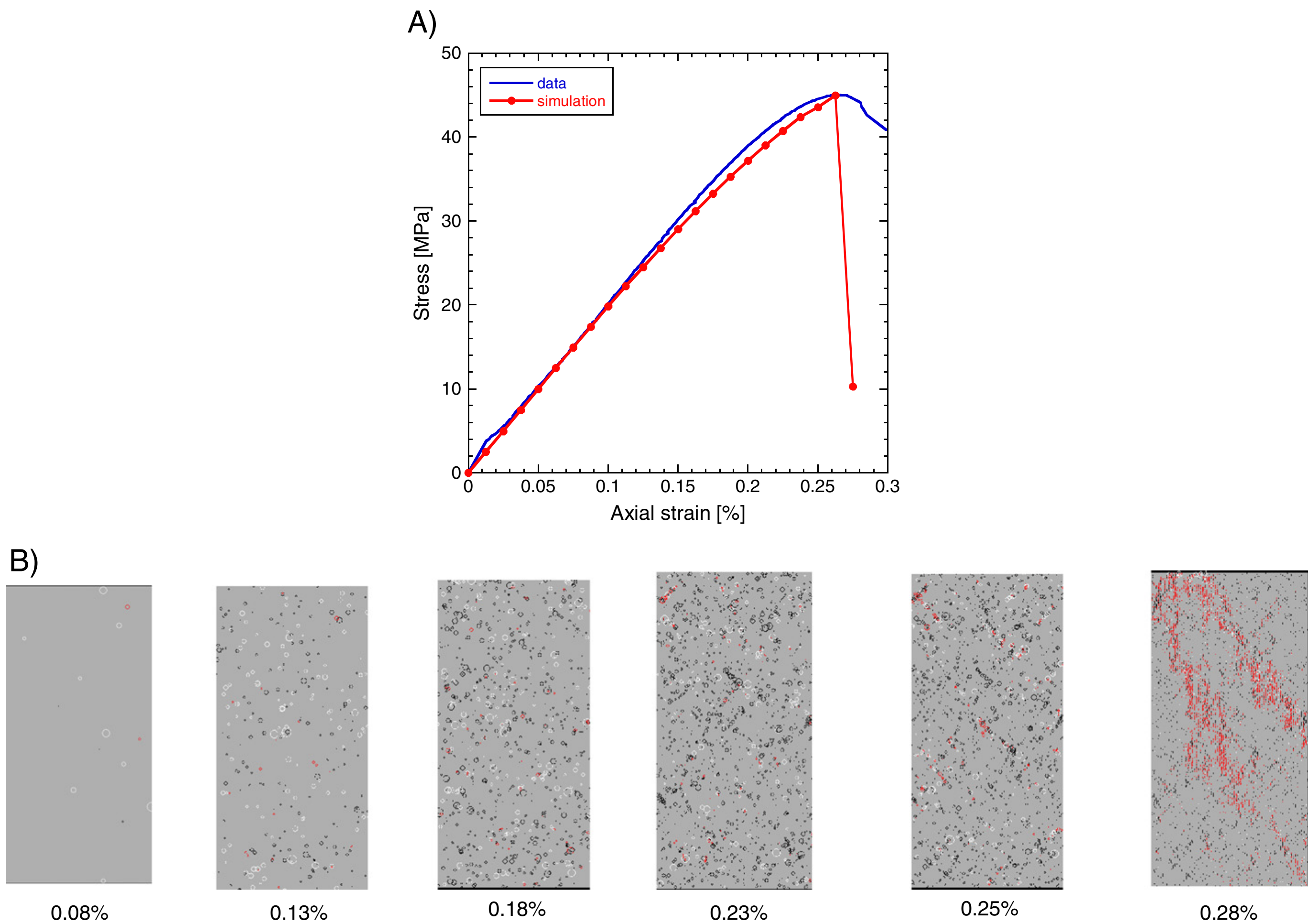

Fig. 13. Results of the simulation for the stylolite free material. (A) Stress as a function of axial strain for a stylolite-free sample from layer O3 and for the numerical simulations. The parameters used in the model are listed in Table 2. (B) Stress-induced damage in the numerical sample. Failure of elements appears red when in tension and black when in shear. Each circle symbol represents one AE event. The size of the circle represents the magnitude of the released energy. (For interpretation of the references to colour in this figure legend, the reader is referred to the web version of this article.)

$K_{IC}\sim 0.2$ MPa m$^{1/2}$, consistent with the measurements of Atkinson and Advis (1980). The prediction of Eq. (2) for different values of the ratio $K_{IC}/\sqrt{\pi r}$ is presented in Fig. 16 and suggests that the pore-size controlling brittle failure in these rocks is, according to the model, around 15 µm. This value is high with respect to our microstructural observations and CT data (Figs. 3 and 4). It is possible that the spatial distribution of microporosity primarily at the periphery of the ooids (Fig. 4) had some influence on the strength of the rocks and this is not taken into account in the model. Regnet et al. (2015b) indeed showed that the mechanical behaviour of microporous oolithic carbonates could be strongly controlled by the microporosity distribution within the grains.

We observed a large water-weakening effect in all the rocks tested, with an average UCS reduction of 34% when compared to the dry samples. Brantut et al. (2014) recently showed that significant time-dependent deformation due to stress-corrosion microcracking could occur in limestone in the presence of water at low strain rates. Considering that the experiments were performed at comparatively higher strain rates, we do not believe that this was a factor here and water-weakening must therefore be related to some time-independent process. Following Eq. (2), it is more likely that this weakening effect is due to a reduction of the fracture surface energy (and consequently of K_{IC}) in the presence of water, as observed in other porous rocks such as sandstone (Baud et al., 2000) and volcanic tuff (Zhu et al., 2011). Our results suggest that the reduction of the fracture surface energy in the presence of water is more pronounced in limestone than in sandstone. Direct measurements of K_{IC} on dry and wet limestones should be performed to confirm this conclusion. Such work is beyond the scope of this study.

7.2. Impact of stylolites on strength

Our new data compiled in Fig. 17 show an average reduction of UCS of 28% for a sample containing a stylolite. This reduction was however quite variable and was found to be in the range 10 to 60%. Since the studied stylolites were closed, we can consider these numbers as lower bounds for the expected strength reduction associated with the presence of stylolites. The obvious conclusion is that impact of stylolites on the strength of carbonate rocks cannot be neglected in various geophysical and geotechnical applications, even if the stylolites are closed. Our new data also suggests that the origin of this weakening is complex. Larbi (2003) suggested that stylolites have a weakening effect as they allow water to penetrate the rock and dissolve some of the constituents of the stylolites, or cause them to swell. However, the results presented in Fig. 8 show a similar reduction in strength for both dry and wet samples, ruling out clay swelling as a factor in our experiments. One unexpected result is the fact that the stylolite orientation had little impact on the magnitude of the strength reduction. One possible explanation

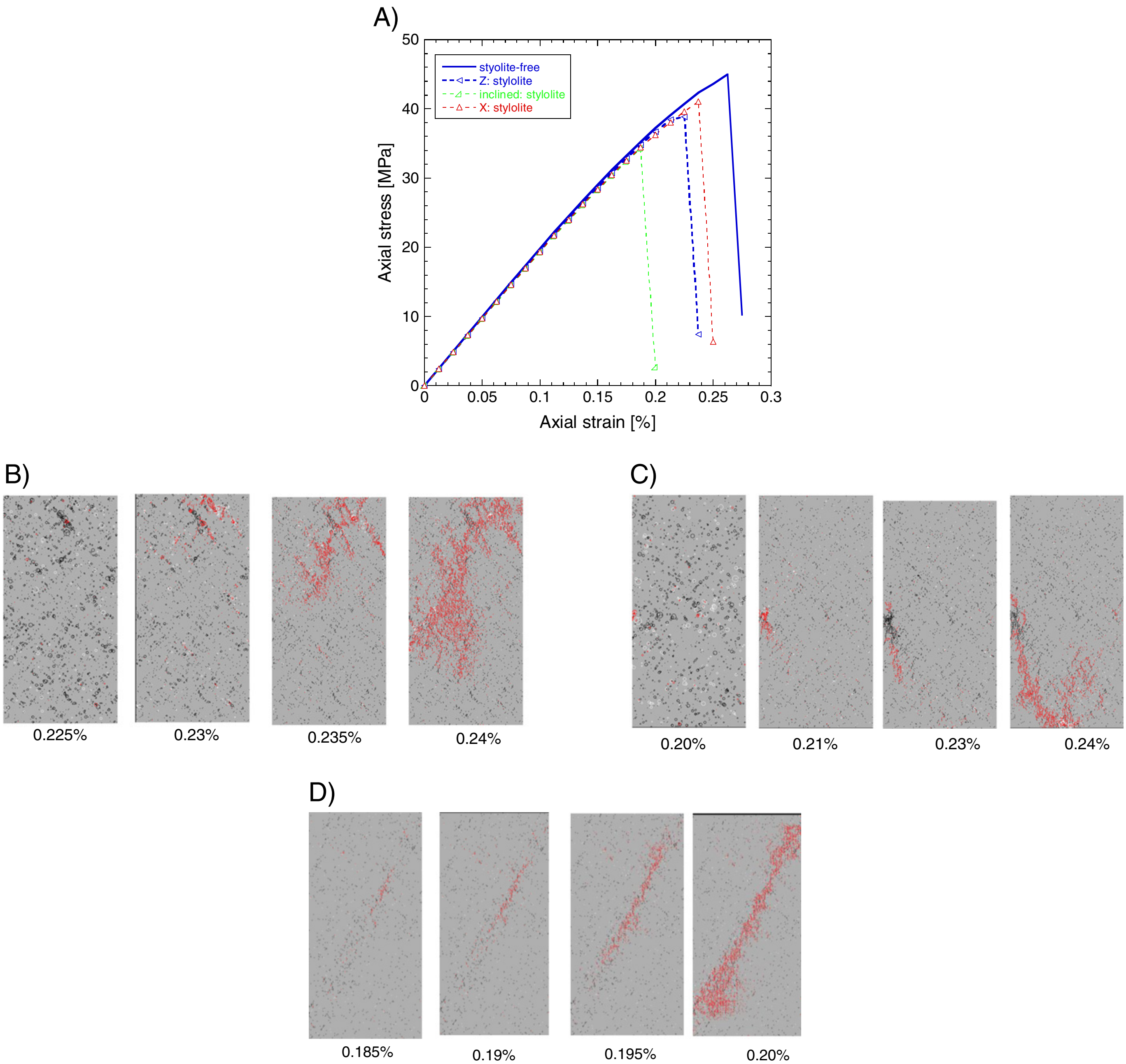

Fig. 14. Results of Simulations 1 for a sample with a stylolite (Fig. 11B–D). (A) Stress as a function of axial strain as predicted by the simulations with a 10% weaker stylolite zone. The parameters used in the model are listed in Table 2. Stress-induced damage in the numerical samples with stylolite oriented orthogonal (B), oblique (C) and (D) parallel to the applied stress (vertical). Failure of elements appears red when in tension and black when in shear. Each circle symbol represents one AE event. The size of the circle represents the magnitude of the released energy. (For interpretation of the references to colour in this figure legend, the reader is referred to the web version of this article.)

would of course be that the stylolites, because they were very thin, did not particularly influence the mechanical behaviour of the sample and that what was observed was only due to some petrophysical differences in the vicinity of these structures, either of pre-stylolization origin or in relation to the stylolite nucleation and growth. Rustichelli et al. (2012) in particular showed that there might be differences in the type and amount of cement in the vicinity of the stylolites. However, some of our numerical simulations (Simulations 1) showed that it is unlikely to be that simple. Moreover, let us consider that the host rock has a porosity and pore radius of ϕ_h and r_h, and that porosity and pore radius around the stylolite is larger: ϕ_s and r_s, respectively. Assuming for simplicity that the whole sample with a stylolite has these different microstructural attributes, the pore-crack model would predict, assuming that the toughness K_{IC} does not change (Eq. (2)), a strength reduction R of

$$R = \frac{UCS^s}{UCS^h} = \left(\frac{\phi_h}{\phi_s}\right)\sqrt{\frac{r_h}{r_s}} \tag{3}$$

With the measured porosity differences, Eq. (3) shows that an increase in pore radius by more than a factor 2 would be needed to find R in the measured range. Since only a small volume around the stylolite appeared to have different properties—a higher porosity (Fig. 6A) and a larger pore-throat size (Fig. 6B)—it is clear that the stylolite as a structure had a major influence on stress-induced damage in the samples. This is essentially what we see in our numerical simulations.

The conclusion is that the strength reduction and failure modes observed in the presence of stylolites are mostly due to the addition of two

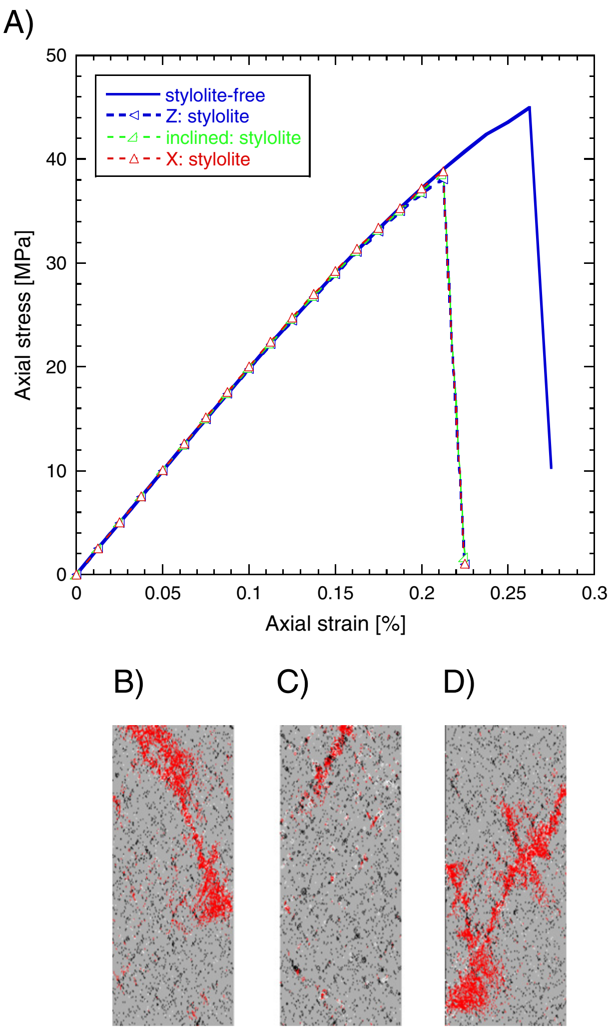

Fig. 15. Results of Simulations 2 for a sample with a rough stylolite (see Fig. 12E–F). (A) Stress as a function of axial strain as predicted by the simulations with a 10% weaker stylolite. The parameters used in the model are listed in Table 2. Stress-induced damage in the numerical samples with stylolite oriented orthogonal (B), oblique (C) and (D) parallel to the applied stress (vertical). Failure of elements appears red when in tension and black when in shear. Each circle symbol represents one AE event. The size of the circle represents the magnitude of the released energy. (For interpretation of the references to colour in this figure legend, the reader is referred to the web version of this article.)

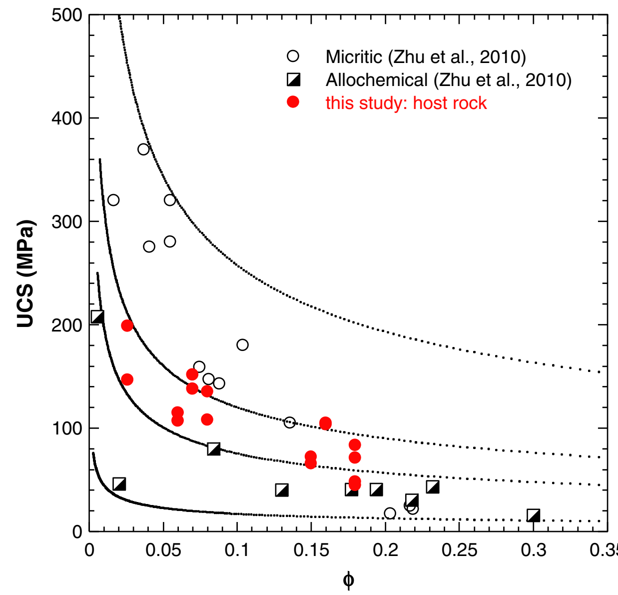

Fig. 16. Comparison of theoretical predictions with laboratory data on unconfined compressive strength (UCS) of micritic (triangles)and allochemical (squares) limestones compiled by Zhu et al. (2010) and the carbonates from Bure (red circles). Theoretical curves of UCS as a function of porosity for four different values of $K_{IC}/\sqrt{\pi r}$ are plotted. (For interpretation of the references to colour in this figure legend, the reader is referred to the web version of this article.)

effects: more porous and therefore weaker material inside and in the vicinity of the stylolite and, the heterogeneity of the stylolite acts as a stress concentrator. Because the roughness of the stylolite has an important role in the development of damage, as suggested by our simulations (Fig. 15), this parameter is probably the reason why some scattering was observed in the experimental UCS data. Spatial variation of the stylolite roughness would indeed promote such variability because a significant difference would then exist between the samples prepared from different parts of the cores. We believe that stochastic modelling was probably the best approach to study this problem because of the inherent differences between the natural samples.

Additional complexity could also arise from the presence of microcracks around the stylolite. However, we believe that such microcracking would mostly enhance the porosity/strength differences between the stylolite and the host rock, which will not significantly change the results presented in Section 6. This was checked through several series of simulations.

7.3. Stylolites: planes of weakness in carbonate formations?

The existence of a plane weakness in a rock implies that the rock is weaker in some orientation (Jaeger et al., 2007). Many examples showed that the brittle strength of rocks is strongly influenced by various geological features such as joints and faults (Bandis et al., 1983; Pollard and Aydin, 1988), and structural heterogeneities such as bedding in sedimentary rocks or cleavage in slates, and preferred orientation and/or arrangement of minerals and cracks in igneous and metamorphic rocks (Donath, 1964; Vernik et al., 1992; Baud et al., 2005). In most of these cases, a degree of mechanical anisotropy is observed. In a foliated rock such as gneiss, a minimum strength is usually observed when the foliation plane is orientated at 45° with respect to the major principal stress (Shea and Kronenberg, 1993; Rawling et al., 2002). Similar observations were also reported on shales (Niandou et al., 1997). Anisotropic shear strength was also observed in concrete replicas of two natural granite joints (Jing et al., 1992). In porous sandstone, significant anisotropy can also be associated with sedimentary bedding. For this case, brittle strength decreases relatively continuously between two end-member situations: the rock deformed perpendicular to bedding has the maximum strength and the rock deformed parallel to bedding has the minimum strength (Dunn et al., 1973; Gatelier et al., 2002; Bésuelle et al., 2003; Louis et al., 2009). There is paucity of data on the mechanical anisotropy of limestone, but our new data on the rocks from Bure show that the stylolite-free material is to the first order isotropic. This is also supported by permeability and P-wave velocity measurements on the same rocks (Rolland, 2013; Heap et al., 2014a).

Our new data on the impact of stylolites appears to contradict field/quarry based observations that exposed stylolites as planes of weakness in carbonate formations. The limited data set of Rashed and Sediek (1997) also suggests that the stylolites induced some anisotropy with minimum strength at ~45° to the applied stress. The numerical simulations presented in the previous section do not suggest that the presence of microcracks around or in the stylolites would change the observed behaviour and explain the differences between our results and the

Please cite this article as: Baud, P., et al., Impact of stylolites on the mechanical strength of limestone, Tectonophysics (2016), http://dx.doi.org/10.1016/j.tecto.2016.03.004

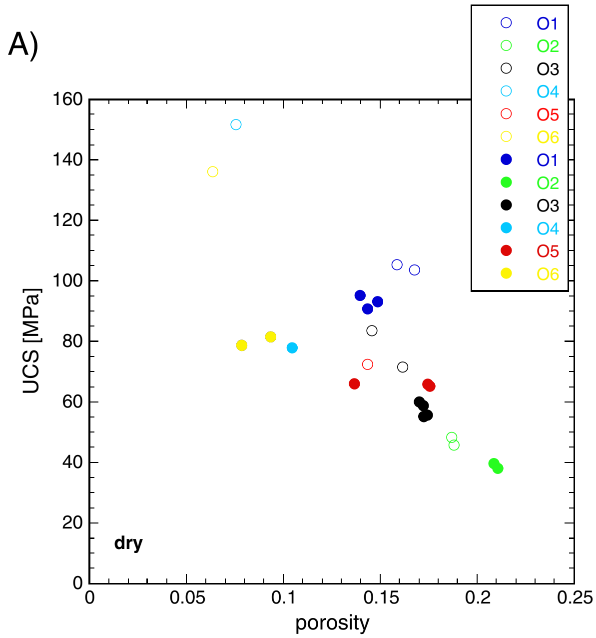

Fig. 17. Compilation of UCS data on samples with a stylolite (closed symbols) and stylolite-free (open symbols): (A) nominally dry samples, (B) water saturated samples.

field observations. As noted before, this would most probably just introduce more scattering in the results. A likely more important parameter was the observation made during sample selection from the EST205 borehole cores from Bure: thicker stylolites (with thicknesses larger than 1 cm) were always associated to macrofracturing in the cores (Fig. 18A) and were therefore impossible to test. Moreover, most attempts made to prepare samples with stylolites of thickness larger than 2–3 mm resulted in fractures along the stylolite planes during sample preparation. In the few cases, where the samples did not actually break during preparation, we could always see some macrofractures associated to the stylolite plane (Fig. 18B) and further manipulations of these samples showed that their mechanical strength was dramatically low (Fig. 18C). We therefore believe that the thickness of the stylolites plays a major role on their impact on rock strength. Taken together, our results therefore suggest the following scenario: when stylolites are thin, as in the studied samples, their roughness plays an important role in the mechanical behaviour. Stress concentrations near the larger teeth oriented in the direction of the applied stress promote microcracking in that direction whatever the orientation of the stylolite. This process does not promote the development of mechanical anisotropy as shown in Simulations 2 (Section 6) and these stylolites cannot be considered as planes of weakness. However when the stylolite thickness is of the order of several mm and beyond, what is typically observed is that it becomes less tortuous (Fig. 18A). Then, when loaded, such structure will have the tendency to behave in a similar way than the numerical samples of Simulation 1 and, in turn, the thick stylolites will become obvious planes of weakness and have very low strength when loaded at an angle to their plane.

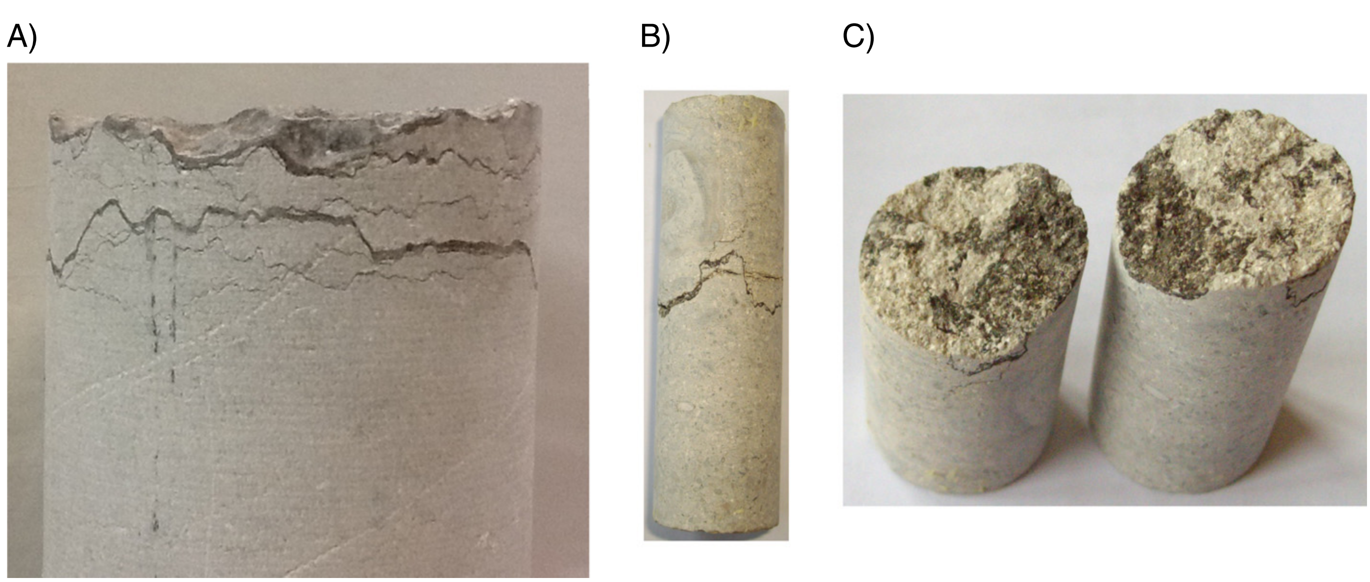

Fig. 18. (A) Photograph of a core from Bure (10 cm diameter). Fracture of this core occurred along a thick stylolite. (B) Photograph of a sample (4 cm × 2 cm) prepared in a zone with a thick stylolite. Preparation induced cracking is visible in part of the stylolite plane. Microcracking made this sample weaker and it broke partially on the stylolite plane (dark zones) during the set-up of the test (C).

8. Conclusions

In this study we showed that a significant strength reduction is expected in the presence of a stylolite, even if there are thin and closed. Such weakening should be taken into account in geotechnical applications, particularly in carbonate formations where stylolites are abundant. Since stylolites are not always developed enough to be identified in carbonate rocks, they also could contribute to the scattering in the petrophysical and mechanical data often reported in this rock type (see for example Dautriat et al., 2011).

When the stylolites are thin, we showed that the observed weakening is about the same for a dry or a wet rock, and also appeared to be the same for different orientations of the stylolite with respect to the applied stress. Most of the observed strength reduction could be explained by the presence of a higher porosity zone in the vicinity of the stylolite. The stylolite itself plays the role of stress concentrator that influences the development of stress-induced damage and failure in the limestone.

Our new data suggest that stylolites would become planes weakness in carbonate formations beyond a certain thickness. Our observations suggest that this thickness is around 5 mm and that a more dramatic weakening is to be expected when the stylolite reaches this thickness. Mechanical tests on such thick stylolites were not possible in this study and we believe that they would be extremely challenging to perform. It is in our view more realistic to envisage some indirect in-situ measurements to quantify strength for thick stylolites and their impact at various scales.

Acknowledgements

Data will be available on demand. This work was partially funded by Andra through a Ph.D. grant for Alexandra Rolland. We thank Stephen Laubach, an anonymous reviewer, and the Associate Editor for thoughtful reviews. We thank Bertrand Renaudié and Jean-Daniel Bernard for their very delicate work on the sample preparation. The mercury porosimetry was performed at the University of Aberdeen and thanks go to Dave Healy and Colin Taylor. We thank Gilles Morvan for his assistance on the SEM. The paper has benefitted from discussions with Philippe Landrin, François Renard, and Teng-fong Wong. Tao Xu acknowledges the National Natural Science Foundation of China (grant number 51474051, 41172265), the National Basic Research Programme of China (grant number 2013CB227900), and the Fundamental Research Funds for the Central Universities of China (grant number N130501002, L1501004).

References

André, G., 2003. Caractérisation des déformations méso-cénozoïques et des circulations de fluides dans l'est du Bassin de Paris, thesis. Univ, Henri Poincaré, Nancy, France.
Atkinson, B.K., Advis, V., 1980. Fracture mechanics parameters of some rock-forming minerals determined using an indentation technique. Int. J. Rock Mech. Min. Sci. & Geomech. Abst. 17, 383–386.
Bandis, S.C., Lumsden, A.C., Barton, N.R., 1983. Fundamentals of rock joint deformation. Int. J. Rock Mech. Min. Sci. 20 (6), 249–268.
Baron, M., Parnell, J., 2007. Relationships between stylolites and cementation in sandstone reservoirs: examples from the North Sea. U.K. and East Greenland. Sed. Geol. 194 (1–2), 17–35.
Bathurst, R.G.C., 1971. Carbonate Sediments and Their Diagenesis. Elsevier, Amsterdam/London/New York.
Baud, P., Wong, T.-f., Zhu, 2014. Effects of porosity and crack density on compressive strength of rocks. Int. J. Rock Mech. Min. Sci. 67, 202–211.
Baud, P., Zhu, W., Wong, T.-f., 2000. Failure mode and weakening effect of water on sandstone. J. Geophys. Res. 105, 16371–16390.
Baud, P., Louis, L., David, C., Rawlings, G.C., Wong, T.-f., 2005. Effects of bedding and foliation on mechanical anisotropy, damage evolution and failure mode. Geophys. Soc. London Spec. Pub. 245, 223–249.
Bésuelle, P., Baud, P., Wong, T.-f., 2003. Failure mode and spatial distribution of damage in Rothbach sandstone in the brittle–ductile transition. Pure Appl. Geophys. 160, 851–868.
Braithwaite, C.J.R., 1989. Stylolites as open fluid conduits. Mar. Pet. Geol. 6, 93–96.
Brantut, N., Heap, M.J., Baud, P., Meredith, P.G., 2014. Mechanisms of time-dependent deformation in porous limestone. J. Geophys. Res. 119 (7), 5444–5463.
Cilona, A., Baud, P., Tondi, E., Agosta, F., Vinciguerra, S., Rustichelli, A., Spiers, C.J., 2012. Deformation bands in porous carbonate grainstones: field and laboratory observations. J. Struct. Geol. 45, 137–157.
Cilona, A., Faulkner, D.R., Tondi, E., Agosta, F., Mancini, L., Rustichelli, A., Vinciguerra, S., Baud, P., 2014. The effects of rock heterogeneity on compaction localization in porous carbonates. J. Struct. Geol. 67, 75–93.
Croizé, D., Renard, F., Gratier, J.-P., 2013. Chapter 3—compaction and porosity reduction in carbonates: a review of observations, theory and experiments. Adv. Geophys. 54, 181–238.
Dautriat, J., Gland, N., Dimanov, A., Raphanel, J., 2011. Hydromechanical behavior of heterogeneous carbonate rock under proportional triaxial loading. J. Geophys. Res. 116. http://dx.doi.org/10.1029/2009JB000830.
Dawson, W.C., 1998. Stylolite Porosity in Carbonate Reservoirs. AAPG Search and Discovery Article. AAPG Annual Convention, Houston, Texas, 91030.
Donath, F.A., 1964. Strength variation and deformational behaviour in anisotropic rock. In: Judd, W.R.,. (Ed.), State of Stress in the Earth's Crust. American Elsevier, New York, pp. 281–297.
Dunn, D.E., LaFountain, L.J., Jackson, R.E., 1973. Porosity dependence and mechanism of brittle fracture in sandstones. J. Geophys. Res. 78, 2403–2417.
Dunnington, H.V., 1967. Aspects of diagenesis and shape change in stylolitic limestone reservoirs, Proc. World Pet. Congr. 7th. Mexico 2, 339–352.
Ebner, M., Piazolo, S., Renard, F., Koehn, D., 2010. Stylolite interfaces and surrounding matrix material: nature and role of heterogeneities in roughness and microstructural development. J. Struct. Geol. 32 (8), 1070–1084.
Gatelier, N., Pellet, F., Loret, B., 2002. Mechanical damage of an anisotropic porous rock in cyclic triaxial tests. Int. J. Rock Mech. Min. Sci. 39, 335–354.
Heald, M.T., 1955. Stylolites in sandstones. J. Geol. 63 (2), 101–114.
Heap, M.J., Baud, P., Reuschlé, T., Meredith, P.G., 2014a. Stylolites in limestones: barriers to fluid flow? Geology 42 (1), 51–54.
Heap, M., Petrakova, L., Lavallée, Y., Baud, P., Varley, N.R., Dingwell, D.B., 2014b. Microstructural controls on the physical and mechanical properties of edifice-forming andesites at Volcan de Colima, Mexico. J. Geophys. Res. 119. http://dx.doi.org/10.1002/2013JB010521.
Heap, M.J., Xu, T., Chen, C.-f., 2014c. The influence of porosity and vesicle size on the brittle strength of volcanic rocks and magma. Bull. Volcano. 78, 856.
Jaeger, J.C., Cook, N.G.W., Zimmerman, R.W., 2007. Fundamentals of Rock Mechanics. fourth ed. Blackwell, Oxford, p. 475 pp.
Ji, Y., Hall, S., Baud, P., Wong, T.-f., 2015. Characterization of pore structure and strain localization in Majella limestone by X-ray computed tomography and digital image correlation. Geophys. J. Int. 200, 701–719.
Ji, Y., Baud, P., Vajdova, V., Wong, T.-f., 2012. Characterization of pore geometry of Indiana limestone in relation to mechanical compaction. Oil & Gas Science and Technology - Revue de l'Institut Français du Pétrole. http://dx.doi.org/10.2516/ogst/2012051.
Jing, L., Nordlund, E., Stephansson, O., 1992. An experimental study on the anisotropy and stress-dependency of the strength and deformability of rock joints. Int. J. Rock Mech. Min. Sci. Geomech. Abstr. 29, 535–542.
Larbi, J.A., 2003. Effect of stylolites on the durability of building stones: two cases studies. HERON 48 (3).
Lind, I., Nykjaer, O., Priisholm, S., Olie, M., Springer, N., 1994. Permeability of stylolite-bearing chalk. J. Pet. Technol. 46, 986–993.
López-Buendía, A.M., Guillem, C., Cuevas, J.M., Mateos, F., Montoto, M., 2013. Natural stone reinforcement of discontinuities with resin for industrial processing. Eng. Geol. 166, 39–51.
Louis, L., Baud, P., Wong, T.-f., 2009. Microstructural inhomogeneity and mechanical anisotropy associated with bedding in sandstone. Pure Appl. Geophys. 166, 1063–1087.
Nelson, R.A., 1981. Significance of fracture sets associated with stylolite zones. Am. Assoc. Petrol. Geol. Bull. 65, 2417–2425.
Nenna, F.A., Aydin, A., 2011. The formation and growth of pressure solution seams in clastic rocks: a field and analytical study. J. Struct. Geol. 33, 633–643.
Niandou, H., Shao, J.F., Henry, J.P., Fourmaintraux, D., 1997. Laboratory investigation of the mechanical behaviour of Tournemire shale. Int. J. Rock Mech. Min. Sci. 34, 3–16.
Nicholson, D.T., Nicholson, F.H., 2000. Physical deterioration of sedimentary rocks subjected to freeze–thaw weathering. Earth Surf. Proc. Land. 25 (12), 1295–1307.
Özvan, A., Dincer, I., Acar, A., 2011. Quality assessment of geo-materials for coastal structures (Yumurtalik, Turkey). Marine Geores. Tech. 29, 299–316.
Park, W.C., Schot, E.H., 1968. Stylolites: their nature and origin. J. Sed. Petrol. 38 (1), 175–191.
Pires, V., Silva, Z.S., G., Simão, J.A.R., Galhano, C., Amaral, P.M., 2010. "Bianco di asiago" limestone pavement — degradation and alteration study. Construt Build. Mat. 24, 686–694.
Pollard, D.D., Aydin, A.A., 1988. Progress in Understanding Jointing over the Past Century: Geological Society of America Bulletin. 100 pp. 1181–1204.
Raynaud, S., Carrio-Schaffhauser, E., 1992. Rock matrix structures in a zone influenced by a stylolite. J. Struct. Geol. 14, 973–980.
Rashed, M.A., Sediek, K.N., 1997. Petrography, diagenesis and geotechnical properties of the El-Rufuf Formation (Thebes Group), El-Kharga Oasis, Egypt. J. Afr. Earth Sc. 25 (3), 407–423.
Rawling, G.C., Baud, P., Wong, T.-f., 2002. Dilatancy, brittle strength, and anisotropy of foliated rocks: experimental deformation and micromechanical modeling. J. Geophys. Res. 107 (10), 1–14.
Regnet, J.B., Robion, P., David, C., Fortin, J., Brigaud, B., Yven, B., 2015a. Acoustic and reservoir properties of microporous carbonate rocks: implication of micrite particle size and morphology. J. Geophys. Res. http://dx.doi.org/10.1002/2014JB011313.
Regnet, J.B., David, C., Fortin, J., Robion, P., Makhloufi, Y., Collin, P.Y., 2015b. Influence of microporosity distribution on the mechanical behavior of oolithic carbonate rocks. Geomech. En. Env. 3, 11–23.
Rolland, A., 2013. Rhéologie, localisation de la déformation et histoire des contraintes dans les calcaires du site de Bure. Université de Strasbourg, Thèse de doctorat.

Rolland, A., Toussaint, R., Baud, P., Schmittbuhl, J., Conil, N., Koehn, D., Renard, F., Gratier, J.-P., 2012. Modeling the growth of stylolites in sedimentary rocks. J. Geophys. Res. 117 (6), B06403.

Rolland, A., Toussaint, R., Baud, P., Conil, N., Landrein, P., 2014. Morphological analysis of sedimentary stylolites for paleostress estimation in limestones surrounding the Andra Underground Research Laboratory site. Int. J. Rock Mech. Min. Sci. 67, 212–225.

Rustichelli, A., Tondi, E., Agosta, F., Cilona, A., Giorgini, M., 2012. Development and distribution of bed-parallel compaction bands and pressure solution seams in carbonates (Bolognano Formation, Majella Mountain, Italy). J. Struct. Geol. 37, 181–199.

Rustichelli, A., Tondi, E., Korneva, I., Baud, P., Vinciguerra, S., Agosta, F., Reuschlé, T., Janiseck, J.M., 2015. Bedding parallel stylolites in shallow-water limestone successions of the Apulian carbonate platform (central-Southern Italy). Italian J. Geosc. 134 (3), 513–534.

Rutter, E.H., 1983. Pressure solution in nature, theory and experiment. J. Geol. Soc. 140, 725–740.

Sammis, C.G., Ashby, M.F., 1986. The failure of brittle porous solids under compressive stress states. Acta Metall. 34, 511–526.

Schmitt, L., Forsans, T., Santarelli, F.J., 1994. Shale testing and capillary phenomena. Int. J. Rock Mech. Min. Sci. & Geomech. Abstr. 31 (5), 411–427.

Schmittbuhl, J., Renard, F., Gratier, J.P., Toussaint, R., 2004. Roughness of stylolites: implications of 3D high resolution topography measurements. Phys. Rev. Lett. 93 (23), 238501. http://dx.doi.org/10.1103/PhysRevLett.93.238501.

Shea, W.T., Kronenberg, A.T., 1993. Strength and anisotropy of foliated rocks with varied mica contents. J. Struct. Geol. 15, 1097–1112.

Stockdale, P.B., 1943. Stylolites: primary or secondary? J. Sediment. Petrol. 13, 3–12.

Tang, C., 1997. Numerical simulation of progressive rock failure and associated seismicity. Int. J. Rock Mech. Min. Sci. 34, 249–261.

Vajdova, V., Zhu, W., Chen, T.-M.N., Wong, T.-f., 2010. Micromechanics of brittle faulting and cataclastic flow in Tavel limestone. J. Struct. Geol. 32, 1158–1169.

Vajdova, V., Baud, P., Wu, L., Wong, T.-f., 2012. Micromechanics of inelastic compaction in two allochemical limestones. J. Struct. Geol. 43, 100–117.

Vernik, L., Lockner, D., Zoback, M.D., 1992. Anisotropic strength of some typical metamorphic rocks from the KTB pilot hole. Germany. Sci. Drill. 3, 153–160.

Weibull, W., 1951. A statistical distribution function of wide applicability. J. Appl. Mech. 18, 293–297.

Wong, T.-f., Wong, R.H.C., Chau, K.T., Tang, C.A., 2006. Microcrack statistics, Weibull distribution and micromechanical modeling of compressive failure in rock. Mech. Mat. 38, 664–681.

Xu, T., Tang, C.-a., Zhao, J., Li, L., Heap, M.J., 2012. Modelling the time-dependent rheological behavior of heterogeneous rocks. Geophys. J. Int. 189, 1781–1796.

Yates, T.J.S., Chakrabarti, B., 1998. Stone Cladding Panels: In-Sity Weathering. CRC Press.

Zhou, X., Aydin, A., 2010. Mechanics of pressure solution seam growth and evolution. J. Geophys. Res.-Solid Earth 115, 18.

Zhu, W., Baud, P., Wong, T.-f., 2010. Micromechanics of cataclastic pore collapse in limestone. J. Geophys. Res. 115, B04405. http://dx.doi.org/10.1029/2009JB006610.

Zhu, W., Baud, P., Vinciguerra, S., Wong, T.-f., 2011. Micromechanics of brittle faulting and cataclastic flow in Alban Hills Tuff. J. Geophys. Res. 106. http://dx.doi.org/10.1029/2010JB008046.

Please cite this article as: Baud, P., et al., Impact of stylolites on the mechanical strength of limestone, Tectonophysics (2016), http://dx.doi.org/10.1016/j.tecto.2016.03.004